

Advanced Electron Energy Loss Spectroscopy for Battery Studies

Zu-Wei Yin, Wenguang Zhao, Jianyuan Li, Xin-Xing Peng, Cong Lin,* Mingjian Zhang, Zhiyuan Zeng, Hong-Gang Liao, Haibiao Chen, Hai Lin,* and Feng Pan*

As a powerful tool for chemical compositional analyses, electron energy loss spectroscopy (EELS) can reveal an abundance of information regarding the atomic-level electron state in a variety of materials, including the elemental types as well as their valence and concentration distributions, and the structure-related atom radial distribution. Benefiting from its unique capabilities and the newly developed advanced transmission electron microscope (TEM) configurations (i.e., in situ bias, in situ heating, cryo-TEM, etc.), EELS has facilitated the battery studies in various aspects. Here, a brief introduction of EELS is provided. Thereafter, a description of the recent progress in studying battery materials using EELS is provided, and finally a look ahead on the future development of EELS techniques and their applications in battery studies is provided.

1. Introduction

Owing to the benefits such as high energy density, high operating voltage, long cycle life, and environmental friendliness, rechargeable batteries have become the foremost means of electric energy storage for electronics and transportation. The structural and compositional evolutions of the key components including electrodes, electrolytes, and interphases must be studied for pursuing high-performance batteries.^[1]

Z.-W. Yin, W. Zhao, J. Li, C. Lin, M. Zhang, H. Lin, F. Pan School of Advanced Materials Peking University Shenzhen Graduate School Shenzhen 518055, P. R. China E-mail: lincong@pku.edu.cn; linhai@pkusz.edu.cn; panfeng@pkusz.edu.cn X.-X. Peng, H.-G. Liao State Key Lab of Physical Chemistry of Solid Surface College of Chemistry and Chemical Engineering Xiamen University Xiamen 361005, P. R. China Z. Zeng Department of Materials Science and Engineering City University of Hong Kong Hong Kong 999077, P. R. China H. Chen Institute of Marine Biomedicine Shenzhen Polytechnic Shenzhen 518055, China

The ORCID identification number(s) for the author(s) of this article can be found under https://doi.org/10.1002/adfm.202107190.

DOI: 10.1002/adfm.202107190

Electron energy loss spectroscopy (EELS), which is now extensively equipped inside the transmission electron microscope (TEM) to provide useful atomic-level information on the elemental types with their valence and concentration distributions, and the structure-related atom radial distribution, has already been validated as a very effective tool in studying the battery materials.^[2] In comparison, other alternative techniques with similar functions, i.e., X-ray photoelectron spectroscopy (XPS), X-ray absorption spectroscopy (XAS), Raman spectroscopy, inductively coupled plasma-mass spectroscopy (ICP-MS), may only give limited and average information from the

sample surface at a large micro-scale or are difficult to be conducted in situ.^[3]

In recent years, several advanced TEM/EELS configurations, including the various types of in situ bias, in situ heating, and cryo-TEM, have been developed. These configurations have allowed for the successful observations of some previously unknown structural and compositional evolutions, such as the nanoscale solid electrolyte interphase (SEI) on the Li metal, cathode electrolyte interphase (CEI) on the layered oxides, Li K-edge evolution, thermal-induced material degradation, and metal-valence distribution evolution in electrodes during charge/discharge, etc. [4]

In consideration of the widespread applications and significant achievements of EELS in battery research, there is now a serious shortage of the reviews and perspectives focusing on the battery chemistries studied by EELS. To our knowledge, the existing reviews/perspectives on the TEM studies in batteries mostly focus on the crystal structure evolutions unveiled by imaging.^[5] There have also been some reviews about the battery studies using the X-ray based techniques with functionalities comparable to EELS, but these techniques are incapable of providing the local information at the nano/atomicscale.^[6] For EELS, although there are several reviews published, they only focus on the methodology, such as the surface plasmons characterization, [7] EELS tomography, [8] high spatial and energy resolution EELS,[9] etc. In comparison, this review comprehensively covers the unique EELS capabilities that are different from other characterization alternates, as well as some newly advanced configurations developed for EELS, widespread applications of EELS in material-related fields, and some recent work utilizing EELS in battery studies. We believe that it will spark fresh ideas for employing EELS to probe the battery materials.

ADVANCED FUNCTIONAL MATERIALS

16163028, 2022, 1, Downloaded from https

elibrary wiley.com/doi/10.1002/adfm.2021/07190 by University Town Of Shenzhen, Wiley Online Library on [24/11/2025]. See the Terms and Conditions (https://onlinelibrary.wiley.com/terms-and-conditions) on Wiley Online Library for rules of use; OA articles are governed by the applicable Cerative Commons

www.advancedsciencenews.com www.afm-journal.de

Table 1. Comparisons of EELS with other characterization techniques. [2,3,4b-d,10]

Techniques	Working principle	Signal acquisition	Spatial resolution	Detecting depth	Capabilities
EELS	Inelastic scattering of incident electrons with samples	Transmission electrons	Atomic level	≈100 nm	Elemental types, valence state (0–5 keV), valence and concentration distributions, ratio of different elements, coordination environment, chemical bond, RDF
Soft XAS	Inelastic scattering of incident X-ray Photons with samples	Secondary electrons/ fluorescence	≈1 µm	5–10 nm for TEY, ≈100 nm for TFY	Elemental types, valence state (200–2000 eV), coordination environment, Electron spin state
Hard XAS	Inelastic scattering of incident X-ray photons with samples	Fluorescence/transmission photons	≈1 µm	≈µm level	Elemental types, valence state (2–20 keV), RDF
XPS	Inelastic scattering of incident X-ray photons with samples	Secondary electrons	≈1 µm	1–5 nm	Elemental types, Valence state, Chemical bond
TXM	Inelastic scattering of incident X-ray photons with samples	Transmission photons	20–30 nm	≈100 nm	Elemental type, valence state (200–2000 eV), valence distribution, coordination environment,
EDX	Excitation of elemental charac- teristic X-ray photons by incident electrons	Elemental characteristic X-ray photons	Atomic level	<1 µm	Elemental types, element concentration distribution, ratio of different elements
NS	Elastic/inelastic scattering of incident neutrons with samples	Scattering neutrons	≈l mm	> 100 mm	Coordination environment, RDF
FTIR	Adsorption of incident infrared ray photons by samples	Transmission or reflection infrared ray photons	≈l µm	5–10 nm	Chemical bond
Raman	Inelastic scattering of incident photons with samples	Scattered Raman photons (by transmission or reflection)	≈l µm	5–10 nm	Chemical bond
ICP-MS	Molecular dissociation to achieve <i>m/z</i> value	m/z value	/	1	Elemental type, ratio of different elements

2. Unique Capabilities of EELS

As listed in Table 1, typical chemical compositional analyses for the battery studies include the electron-based techniques (e.g., EELS, energy dispersive X-ray spectroscopy (EDX), etc.), X-ray based techniques (i.e., XPS, XAS (including both soft and hard), TXM (transmission X-ray microscopy), etc.), neutron scattering (NS), Raman spectroscopy, Fourier transform infrared spectroscopy (FTIR), ICP-MS, etc.^[3] When comparing these techniques, it can be observed that EELS possesses obvious advantages over others. 1) EELS has the most comprehensive capabilities, including characterizing the elemental types, valence state, valence and concentration distributions, ratio of different elements, coordination environment, chemical bond and radial distribution function (RDF), while other techniques (e.g., XAS, TXM, Raman, etc.) only have part of such functions.^[10] 2) EELS shows the highest spatial resolution at atomic level, which benefits from the recent advances in the monochromators, direct electron detectors, and spherical aberration correctors, [11] while XPS, XAS (both hard and soft X-ray), NS, Raman, and FTIR can only provide average information at micro-scale due to the low spatial coherence of X-ray, neutron, and infrared ray, etc. For the X-ray based imaging technique of TXM, it exhibits a spatial resolution of 20-30 nm.^[12] 3) EELS can provide the bulk material information (detecting depth of ≈100 nm), while Raman spectroscopy, FTIR, XPS, and soft X-ray in the total electron yield (TEY) mode can only offer the surface information (detecting depth of < 10 nm) because of the low incident energy. 4) Among

all the techniques that can be used to characterize valence states (i.e., EELS, XPS, XAS, TXM), EELS is the only one possessing the capability to detect the low energy region (e.g., < 100 eV), which makes it the one-of-a-kind tool for identifying the light elements like Li. Besides, although EDX can deliver the atomic-level elemental mapping information in the similar way that EELS does, the electronic structures, coordination numbers, bonding states, and band gaps are unfortunately unavailable, in addition to the lower quantification accuracy than EELS due to the low-energy (<1 keV) X-ray absorption.^[6] Compared with EDX, EELS also possesses a substantially higher collection efficiency, implying that it can be operated at a lower dose to minimize the beam damage. [10] For XAS, it can provide almost the same functions as those of EELS when the soft and hard XAS are combined. For example, the extend X-ray adsorption fine structure (EXAFS) of the hard XAS can also offer the RDF function similar to the extended energy-loss fine structure (EXELFS) of EELS. However, XAS is rather difficult to be available and also more expensive as it requires huge and specialized equipment to speed the electrons. In contrast, EELS is more flexible and can be easily accessed in the laboratory TEM. In addition, because the incident energy of XAS and EELS is just 5-20 keV, whereas that of the electron diffraction is 200-300 keV, EELS can be combined with the electron diffraction to achieve RDF with atomic-level spatial resolution. ICP-MS are difficult to operate in situ and to directly observe the bulk changes. In comparison, EELS can be in situ conducted and allows the materials to be studied beyond nanoscale. [2,4b-d]

16163028, 2022, 1, Downloaded from https

library.wiley.com/doi/10.1002/adfm.202107190 by University Town Of Shenzhen, Wiley Online Library on [24/11/2025]. See the Terms and Conditions (https://onlinelibrary.wiley

and-conditions) on Wiley Online Library for rules of use; OA articles are governed by the applicable Creative Commons

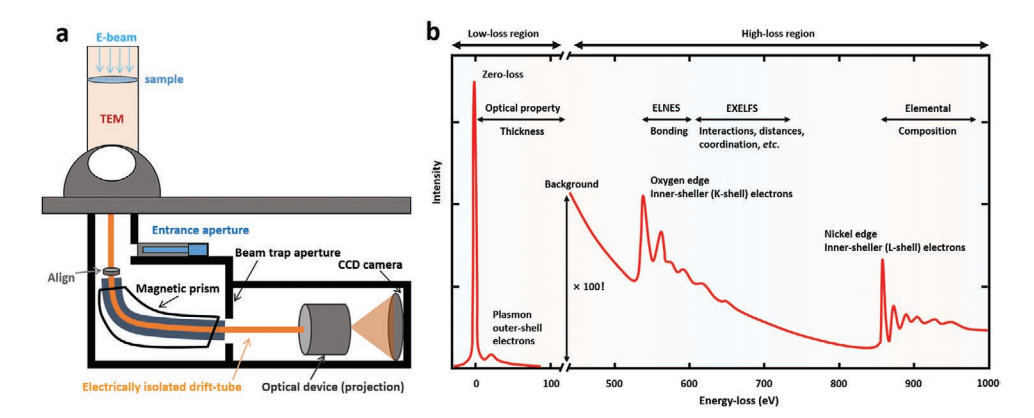


Figure 1. Setup and typical data of EELS. a) Schematic illustration of the typical EELS setup. b) Scheme showing the typical EELS data and the meaning of different peak positions. Reproduced with permission.^[13] Copyright 2011, Springer.

Figure 1a schematically shows the typical postcolumn EELS setup, in which the electrons received by the EELS detector can reflect the material information.^[10] Presently, the EELS instrument is commonly employed in conjunction with a TEM or scanning transmission electron microscope (STEM) to provide microscopic local or even atomic-level information. In the TEM, the electrons generated by the thermionic or field emission gun are accelerated by the anode inside the acceleration tube and then interact with the specimen. During the process when the incident electrons transmit the specimen, some electrons can interact with the atom nuclei or the atomic electrons. And based on the energy changing, these interactions can be classified as either elastic or inelastic scattering. Elastic scattering happens when the incident electrons interact with the nuclei without electron energy loss (not considering the largerangle scattering, especially the head on collisions), which is widely used in the diffraction- and imaging-based techniques in TEM. When the accelerated electrons interact with the atomic electrons through the Coulomb force, a specific energy loss of the incident electrons occurs as the inelastic scattering, due to the excitation of the atomic electrons to the higher quantum number Bohr orbitals. After transmitting the specimen, the outgoing electrons including the transmission electrons, elastic scattering electrons, and inelastic scattering electrons will be focused by the in-column or postcolumn magnetic prism, where they will be separated and focused at different positions and further recorded by the electron detectors/cameras due to their energy difference. Therefore, the EELS will be achieved and visualized when comparing the energies between the incident and outgoing electrons. And in a typical EELS spectrum (Figure 1b), [13] the zero-loss peak is formed by the transmission and elastically scattered electrons; the valance loss is caused by the excitation of the valance electrons to the conduction band; the plasmon peak is generated by the longitudinal wave-like oscillations of the weak bound electrons; the ionization edge is resulted from the core-shell electrons to the empty state. Further in the practice, the valance loss can be used as the finger print to determine the compounds; the plasmon peak combined with the zero-loss peak is efficient to calculate the specimen thickness; the ionization edge is commonly employed to identify the elemental types as well as their electronic states. Especially for the 3d transition metal elements, the so-called

"white line" caused by the not fully occupied 3d orbitals is quite sensitive to the element states, which can be easily interpreted in most cases by analyzing the edge position or the L_3/L_2 peak ratio (after deconvolution) (right line in Figure 2a). More details of the EELS working principle have been clarified by Carter e al.[10] and Egerton.[13]

Thanks to its high spatial resolution, EELS is thus widely adopted to probe the chemical difference between the material surface and bulk. A typical application of EELS in measuring the chemical composition from bulk to surface of layered cathodes is displayed in Figure 2a,[14] and the exemplary atomiclevel elemental (Ni, O, Cr) and valence (Ni2+/Ni3+) distributions achieved by EELS are demonstrated in Figure 2b.[2a] The recently developed 4D STEM-EELS technique can even realize the 3D chemical structure of materials (Figure 2c).^[15] The innovative sensitive detector and fast electron camera substantially enhance the signal-to-noise ratio (SNR) of the high energyloss area, making it achievable for the EXELFS and the RDF analyses. The RDF is also known by the name of the electron pair distribution function (ePDF), which is similar to the X-raybased pair distribution function (PDF), but when combining with electron diffraction, it can provide significantly higher spatial resolution.[16] A typical EELS in the high energy-loss area with corresponding RDF analysis is shown in Figure 2d.[17]

As stated above, such capabilities of EELS make it a one-ofa-kind tool for battery studies. To date, the conventional EELS technique that provides 2D elemental (e.g., Li, Si, O, C, transition metals (TMs), etc. in battery materials), valence, and concentration distribution information, has been frequently employed to analyze the inhomogeneity and chemical structure evolution in battery materials (i.e., cathodes, anodes, solid electrolytes, etc.). [2c,14] However, as far as we know, the battery studies using the innovative 3D EELS tomography and RDF techniques, which have been applied in other nanostructure and defect characterizations, are still scarce. [2b,15]

3. Emerging Advanced EELS Configurations for Battery Studies

In the recent decade, several advanced TEM configurations have been developed for battery studies, including the in situ

www.afm-journal.de

16163028, 2022, 1, Downloaded from https

unlinelibrary.wiley.com/doi/10.1002/adfm.202107190 by University Town Of Shenzhen, Wiley Online Library on [24.112025]. See the Terms and Conditions (https://onlinelibrary.wiley.com/terms-and-conditions) on Wiley Online Library for rules of use; OA articles are governed by the applicable Creative Commons

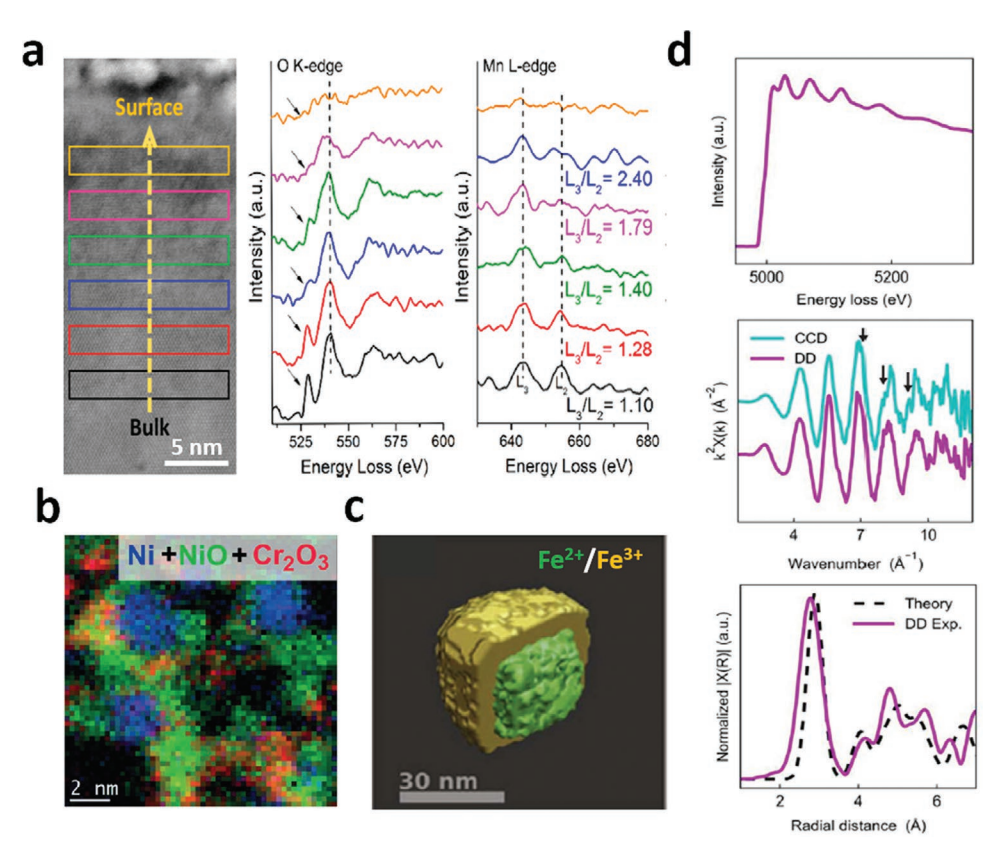


Figure 2. Unique capabilities of EELS. a) Chemical composition analysis of the layered $LiNi_{0.8}Mn_{0.1}Co_{0.1}O_2$ cathode from surface to bulk. Reproduced with permission. American Chemical Society. b) Atomic-level elemental and valence distribution analyses of the $Ni@NiO/Cr_2O_3$ heterostructure. Reproduced with permission. Call Copyright 2015, Wiley-VCH. c) The 3D chemical structural probe of the FeO/Fe₃O₄ core–shell nanocubes. Reproduced with permission. Copyright 2016, American Chemical Society. d) EXELFS and RDF analyses. Reproduced with permission. Copyright 2019, Cambridge University Press.

bias (**Figure 3a**–d), ^[4c,d,18] the cryogenic holder (Figure 3e), ^[19] and the in situ heating (Figure 3f). ^[20] Specifically, the in situ bias rigs include the electrochemical liquid open cell (Figure 3a), ^[4c] the electrochemical solid-state open cell (Figure 3b,d), ^[18] and the electrochemical liquid close cell (Figure 3c). ^[4d] Attributed to them, the TEM imaging and corresponding EELS spectra of battery materials are now achievable not only under different thermodynamics conditions but also in a variety of dynamic environments (e.g., electrochemical solid/liquid or solid/solid systems, heating, cryogenic, etc.).

The probe-type electrochemical open cell using ion liquid as the electrolyte was first demonstrated to study batteries by Huang et al. in 2010, [21] after which it was used and further upgraded by Zhang et al. (Figure 3a). [4c] In Wang and Zhang's setup, the nanoparticles (Li₄Ti₅O₁₂ or FeF₂) loaded on a TEM grid was used as the working electrode, with a Li-coated tungsten tip employed as the counter electrode. [22] Following that, the probe-type electrochemical solid-state open cell (Figure 3b), [18a] the micro-electromechanical system (MEMS)-type electrochemical solid-state open cell (Figure 3c) were developed. [4d] For the first two and the last cell types, solid electrolyte and liquid organic electrolyte were used, respectively. However, for the MEMS-type electrochemical liquid close cell, the thick SiN_x and liquid layers make it practically

impossible for the high-resolution TEM imaging and EELS spectra. $^{[5d,23]}$

The probe-type electrochemical solid-state open cell uses the alkali nitrides/oxides (i.e., Li₂O, Na₂O, etc.) as the solid electrolyte (Figure 3b), [5b,c,18a] which are formed by the nitridation/oxidation of the alkali metals exposed to air, allowing the individual EELS measurements for both the anodes and cathodes. The MEMS-type electrochemical solid-state open cell simulates the real all-solid-state batteries (Figure 3d),[5b,c,18b] and can be utilized to simultaneously observe the anode, cathode, electrolyte, and the interfaces. A similar MEMS-type chip can likewise be employed to conduct the in situ heating with a matching holder (Figure 3f). [20,24] Since 2017, the cryo-TEM has been developed to study the battery materials, with Cui and co-workers being the first to use it.^[19] The cryo-TEM holder's low temperature of <100 K allows the observation of the instable species under the electron beam, such as the Li dendrites, solid electrolyte interphase, etc.[25]

4. Widespread Application of EELS in Material-Related Fields

Due to its distinct advantages over other chemical composition characterization techniques (e.g., XPS, XAS, Raman, ND,

16163028, 2022, 1, Downloaded from https:

onlinelibrary.wiley.com/doi/10.1002/adfm.202107190 by University Town Of Sherzhen, Wiley Online Library on [24/11/2025]. See the Terms and Conditions (https://onlinelibrary.wiley.com/term

and-conditions) on Wiley Online Library for rules of use; OA articles are governed by the applicable Creative Commons

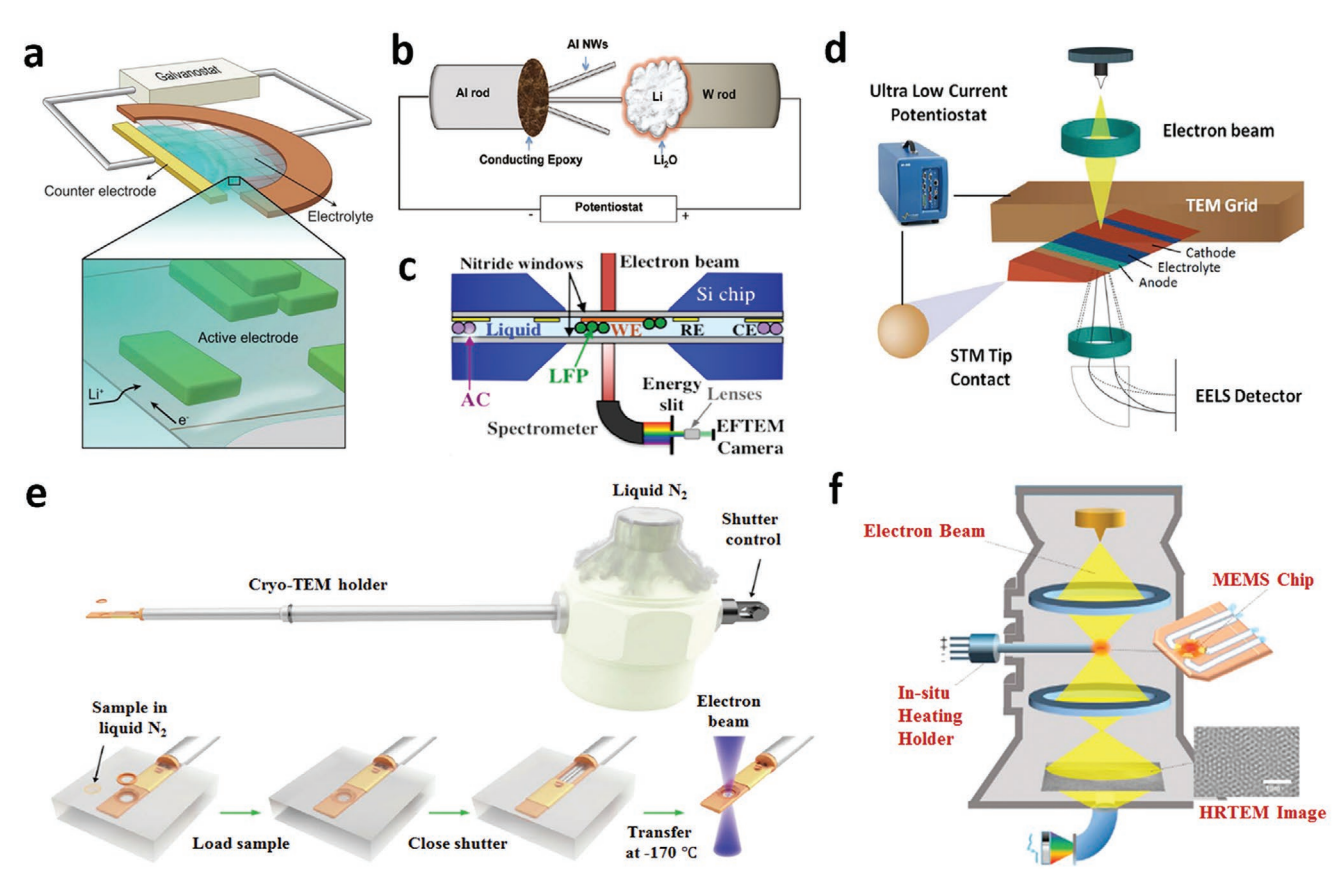


Figure 3. Scheme of the advanced EELS configurations. a) Electrochemical liquid open cell. Reproduced with permission. [4c] Copyright 2020, American Association for the Advancement of Science. b) Probe-type electrochemical solid-state open cell. Reproduced with permission. [18a] Copyright 2011, American Chemical Society. c) Electrochemical liquid close cell. Reproduced with permission. [4d] Copyright 2014, American Chemical Society. d) MEMS-type electrochemical solid-state open cell; Reproduced with permission. [18b] Copyright 2016, American Chemical Society. e) Cryo-TEM holder and the sample preparation process. Reproduced with permission. [19] Copyright 2017, American Association for the Advancement of Science. f) In situ heating set-up. Reproduced with permission. [20] Copyright 2019, Elsevier.

etc.), EELS offers a wide range of applications in various material-related fields, such as nanotechnology, materials/physical chemistry, energy storage and conversion, etc.^[15,26] For instance, EELS can be used to determine the material composition after thermal treatment, [26a] (electro)chemical reactions, [27] strain treatment, [26b] aging, [26d] semiconductor processing, [28] etc., and detect the intermediate states during these processes. [27,29] And with proper configurations, in situ EELS observations can also be conducted. [27,29]

In the material-related fields, the rechargeable battery is a typical complex system since it involves the changes in both the bulk and interface structures, formation of the intermediate products, ion migration, thermal instability, etc.^[3] Similar phenomena have been observed in supercapacitors, (photo)electrocatalysis, corrosion electrochemistry, electrodeposition, etc.,^[30] and thus the advanced EELS configurations employed in the battery studies can also be applied in other fields exhibiting these phenomena. Therefore, reviewing and summarizing the applications of EELS in battery studies is rather significant to both the battery and EELS development, i.e., searching for the innovative methods to explore the battery mechanisms at different scales and the novel EELS application fields.

5. Applications of EELS in Battery Studies

EELS has already promoted the battery understandings with respect to the chemical compositional analyses in the elemental and valence concentrations and radial distribution with high spatial resolution, which has further achieved some important progress in the battery studies when combined with the emerging advanced configurations. This section summarizes some most important applications of EELS in batteries and related achievements, which mainly include five aspects: the battery material composition analyses, intermediate states characterizations, dynamic Li⁺ behaviors, interfacial behaviors, and thermal stability.

5.1. Battery Materials Composition Analyses

For different types of batteries (e.g., Li/Na/Mg/K/Zn-ion,^[32] Li-S,^[33] metal–air,^[34] all-solid-state,^[35] etc.), EELS can explicitly identify their components of the cathodes, anodes, and electrolytes. And the high spatial resolution of EELS also allows for the precise atomic-level element distribution, electron states, and defects. For example, atomic-level EELS and

www.afm-journal.de

16163028, 2022, 1, Downloaded from https

library.wiley.com/doi/10.1002/adfm.202107190 by University Town Of Shenzhen, Wiley Online Library on [24/11/2025]. See the Terms and Conditions (https://onlinelibrary.wiley.com/terms

-and-conditions) on Wiley Online Library for rules of use; OA articles are governed by the applicable Creative Commons

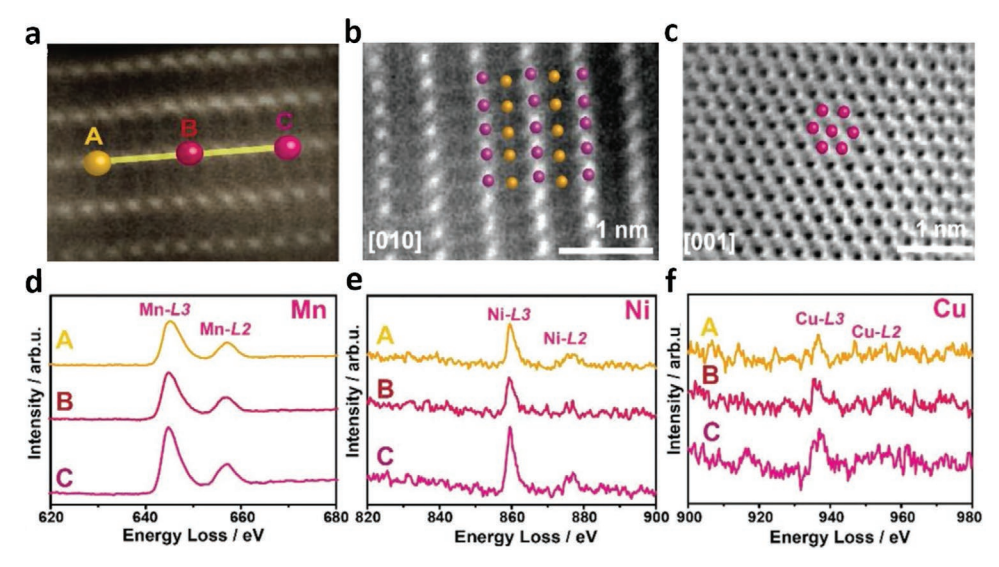


Figure 4. Atomic-level element distribution analyses. a) STEM image and corresponding EELS signals from different elements at various sites d-f). STEM images at the b) [001] zone axis and c) [010] zone axis. Reproduced with permission.^[31] Copyright 2019, Wiley-VCH.

STEM were employed by Xiao et al. to demonstrate the successful synthesis of a novel copper and magnesium co-substituted Na_{2/3}Ni_{1/6}Mn_{2/3}Cu_{1/9}Mg_{1/18}O₂ cathode by confirming the element types at different sites and the crystal structure (Figure 4).[31] Combining EELS and STEM, the structural unit of the prepared material can also be well examined. Nicholls et al. adopted the atomic-level EELS to probe the bonding in the nitrogen-doped graphene (Figure 5a).[36] Carbon atoms surrounding the nitrogen atoms at different sites were identified to explore the effect of the dopant on the electronic state of graphene. In comparison to pure graphene, a shift in the carbon K-edge was observed in the area around the nitrogen atoms, which was ascribed to the C-N bonds. Lee et al. combined atomic-level EELS and first-principle calculations to determine where the Fe antisite defects in the LiFePO₄ cathode came from (Figure 5b). [37] The results revealed that the Li vacancies (V_{1i}) were confined in the 1D channels along the *b*-axis, whose shuttling between the neighboring Fe₁; (Fe at the Li sites) was responsible for the Li/Fe antisite. Guo et al. have also discovered the similar Li/Fe antisite from the EELS and STEM combination.[38]

Coating, doping, and integrated structural modifications at the nanoscale are useful ways to improve the electrochemical performance of battery materials. Compared with other microscale chemical composition characterization techniques (e.g., X-ray based, Raman, ND, etc.), EELS has distinct benefits. Liu et al., for example, utilized TEM imaging, ND, and EELS in the protonated solid electrolyte Li_{6.25}Al_{0.25}La₃Zr₂O₁₂ (LLZO) to quantitatively unveil the individual mobility and lattice occupancy of the H⁺ and Li⁺ ions (Figure 5c-e), [35] and found that a deep ion exchange of Li+ by H+ resulted in a 70 (± 2)% Li loss in the pristine LLZO (Figure 5d). Meanwhile, the noticeable changes in the O K-edge fine structure showed alterations in the O ions' chemical bonding, further confirming the Li+ and H⁺ ion exchange in the LLZO structure.^[35] Using atomic-level EELS/TEM, magnetic susceptibility measurements, and XRD, Guo et al. validated the homogeneous distribution regarding the Mn ions at the Fe sites in the Mn-doped LiFePO₄.^[38] In addition, other researchers have also applied EELS to study the nanocoating carbon on the LiFePO₄,^[39] artificial SEI on the Ni-rich layered oxide,^[40] core–shell Si–C composite,^[41] P2/O3 biphasic layered oxides,^[42] Ni-doped MnO₂,^[43] hollow sulfurrich carbon,^[44] and other battery materials.

5.2. Intermediate State Characterizations

Understanding the battery charge-discharge mechanisms as well as the designs and modifications of high-performance battery materials requires the accurate determination of the intermediates.^[45] For the stable battery materials, the widely used procedure for disassembling the cycled cells proceeds inside a glove box, and the target materials are then moved into a TEM for structural and compositional characterization. Such a simple approach has already achieved many significant findings, such as the phase transition and the metal element segregation during cycling,[27,46] and the reaction mechanisms of metal-air batteries, [47] etc. However, for some instable battery intermediates, the above ex situ characterization is far insufficient. Hence, the in situ electrochemical TEM configurations (liquid/solid-state open cell, liquid close cell, and environmental TEM) were developed, enabling EELS as an efficient technique to perform the operando characterizations of the battery intermediates.

Figure 6a depicts a typical application of EELS in the phase determination of charged LiFePO₄. [48] According to the nanoscale chemical and valence state of each individual Li_xFePO_4 particle probed by EELS, the lithium reactivity cannot be explained by the classical shrinking core model. In different charge states, the studied particle was always observed with the FePO₄ core and the LiFePO₄ shell. [48] The typical lithiation behavior of the conversion-type Fe₃O₄ electrode is shown in Figure 6c. [49] From the results of the XAS and in situ TEM/EELS coupled with the probe-type electrochemical solid-state cell, it

www.afm-journal.de

16163028, 2022, 1, Downloaded from https

elibrary.wiley.com/doi/10.1002/adfm.202107190 by University Town Of Shenzhen, Wiley Online Library on [24/11/2025]. See the Terms

and-conditions) on Wiley Online Library for rules of use; OA articles are governed by the applicable Creative Commons

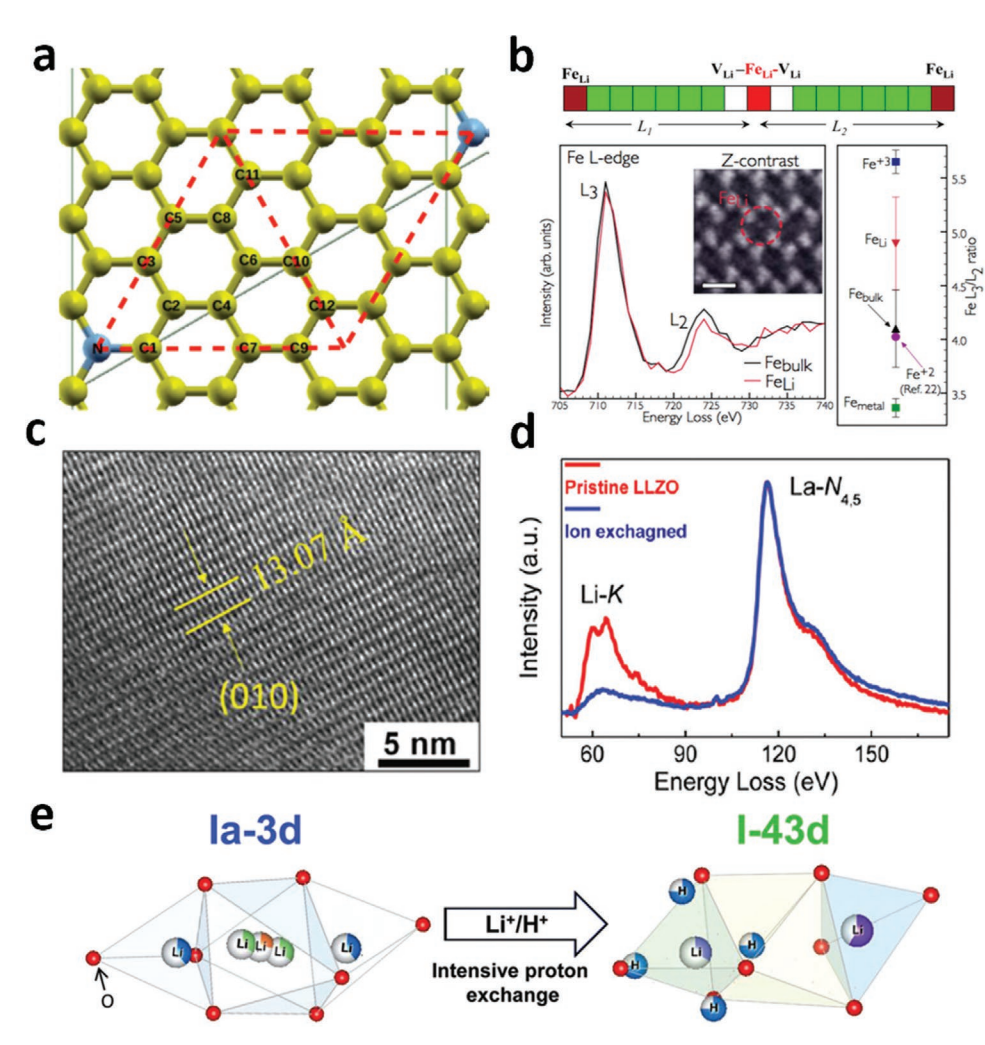


Figure 5. Atomic-level electron states analyses. a) Graphene lattice containing substitutional nitrogen atoms with the unit cell marked by the solid (gray) lines. Reproduced with permission.^[36] Copyright 2019, Wiley-VCH. b) STEM image and corresponding EELS spectrum showing the Li/Fe antisite in the LiFePO₄ cathode. Reproduced with permission.^[37] Copyright 2011, American Physical Society. c–e) STEM image, corresponding EELS spectrum, and schematic showing the Li⁺/H⁺ exchange in the LLZO electrolyte. Reproduced with permission.^[35] Copyright 2019, Royal Society of Chemistry.

was determined that the capacity fading of Fe₃O₄ was a kineticsdependent issue, which was mainly attributed to the formation and augmentation of the passivation layers (internal and surface). Similar phase transformation and phase/metal separation behavior were also observed by TEM/EELS in various electrode materials, such as Co_3O_4 , $^{[50]}$ Fe_2O_3 , $^{[51]}$ sulfur, $^{[46b]}$ overcharged LiCoO₂, $^{[52]}$ Li-rich layered oxides, $^{[53]}$ Li₄Ti₅O₁₂, $^{[54]}$ etc. For the Lirich layered cathodes, EELS has been applied to investigate the injection of the oxygen vacancies into the bulk lattice, which is responsible for the layered-to-spinel phase transformation.^[53b] Ex situ EELS has also been utilized to identify the transition products in the charge-discharge process of the metal-gas batteries, such as the Li-O₂, [55] Li-CO₂, [56] Na-CO₂, [57] Li-CO₂/ O₂,[58] Na-O₂,[59] Na-N₂,[60] etc. Combing the environmental TEM and the probe-type electrochemical solid-state open cell, Huang and co-workers conducted the first in situ TEM/EELS study of a Na-O2 battery (Figure 6b).[59]The oxygen reduction reaction (ORR) of the Au-coated MnO2-nanowire air-cathode was characterized by the NaO2 nanobubbles formed from the Au catalysts, leading to an 18-fold increase in volume on the

MnO₂ nanowire surface, while the EELS results demonstrated that the NaO₂ intermediate was rapidly disproportionated to the Na₂O₂ and O₂, thus resulting in the NaO₂ nanobubble collapse.

In spite of the achievements in detecting the intermediate products by both the ex situ and in situ EELS coupled with the electrochemical solid-state open cells, the operando EELS studies in a liquid cell are still quite challenging. To our best knowledge, there is only one report regarding the in situ EELS study in a liquid cell.[4d] With the valence energy-filtered TEM and the liquid flow cell, for the first time, Holtz et al. successfully utilized the nanoscale EELS to obtain the in situ Li+ distribution mapping of the LiFePO₄ particles in an aqueous electrolyte, which was reflected by the Fe ion distribution (Figure 6d).[4d] In both the solution and the particles, obvious differences between the charged (Figure 6d, medium) and the discharged states (Figure 6d, left and right) were observed in the 5 eV spectroscopic images. When compared with the discharged ones, the charged particles showed brighter regions from the Fe³⁺ ions (indicated by the white arrows in Figure 6d), which corresponded to the delithiated FePO₄. The brightest

www.afm-journal.de

16163028, 2022, 1, Downloaded from https://adv

onlinelibrary.wiley.com/doi/10.1002/adfm.202107190 by University Town Of Shenzhen, Wiley Online Library on [24/11/2025]. See the Terms and Conditions (https://onlinelibrary.wiley.com/terms

-and-conditions) on Wiley Online Library for rules of use; OA articles are governed by the applicable Creative Commons

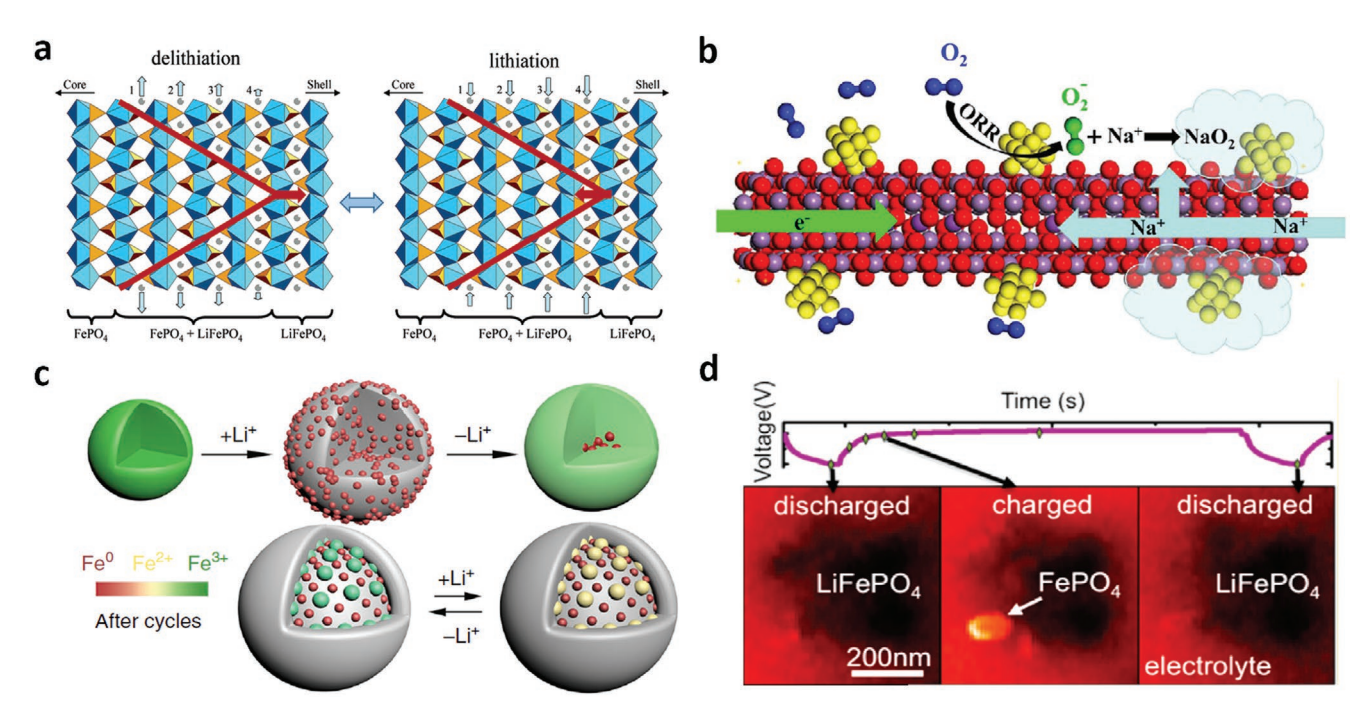


Figure 6. Observations of the intermediate states during the charge–discharge process. a) Schematic views of the interfacial region between the LiFePO₄ and FePO₄ phases. Reproduced with permission. (48) Copyright 2006, American Chemical Society. b) Schematic showing the ORR catalyzed by the Au-coated MnO₂ in the Na–O₂ batteries. Reproduced with permission. (59) Copyright 2019, Elsevier. c) Schematic model depicting the phase evolution of the Fe₃O₄ electrode. Reproduced with permission. (49) Copyright 2019, Nature Publishing Group. d) The 5 eV spectroscopic energy-filtered TEM images. Reproduced with permission. (4d) Copyright 2014, American Chemical Society.

particles represented the FePO₄ that were completely delithiated, while the overall small rise in the intensity may indicate the partially delithiation. These bright FePO₄ regions disappeared upon discharge, suggesting the transition back to the LiFePO₄. These results indicated the competing delithiation mechanisms, including the modes of the core–shell and the anisotropic growth occurring simultaneously for various particles under the same conditions.

5.3. Dynamic Li⁺ Behaviors

Direct observation of the Li⁺ ions inside the operating LIB is of great significance for a better understanding of the battery working mechanisms and issues.^[61] Due to the technical limitations, the energy resolution for Li is relatively poor for the X-ray based technologies (e.g., XPS, XAS, etc.), which makes them almost incapable of the direct Li⁺ observation. Fortunately, EELS is a one-of-a-kind tool for detecting the light Li element.^[62] Utilizing EELS coupled with advanced electrochemical TEM configurations, some researchers have reported the observations regarding the dynamic Li⁺ behaviors during cycling (e.g., migration pathway,^[4c] Li element distribution,^[2c,18b] etc.).

Applying EELS, Hightower et al. performed the first study on the electronic states of the Li-intercalated graphite. [63] Their results indicated that the Li K-edge of the LiC₆ was almost the same as that of the metallic Li, while the C K-edge was only minimally altered by the Li presence. Accordingly, only a few charge transfer from the Li atoms to the C atoms was suggested in the LiC₆, which was opposite to the previous surface XPS

results. Wang et al. investigated the Li chemical distribution and bonding in the intercalated graphite.^[64] The discharged graphite's electronic structure was determined from the nearedge fine structure of the Li and C *K*-edges together with the ab initio calculations. As observed in the high-resolution TEM, direct Li mapping in the graphite disclosed some nanoscale inhomogeneities (i.e., nonstoichiometric regions), which were associated with the local phase separation and structural disorder. Gu et al. used STEM and EELS to successfully observe the atomic-resolution lithium staging in the partially delithiated LiFePO₄. Their results suggested that the residual Li⁺ ions preferred to occupy every second layer along the *b*-axis in the partially delithiated LiFePO₄.^[65] The Li distribution in the discharged Si anode and the core-hole effect in the delithiated LiCoO₂ were also unveiled by EELS.^[2c]

Coupling EELS with the electrochemical liquid open cell, Zhang et al. firstly realized the real-time monitoring of the Li⁺ kinetic pathways in the fast-charging Li₄Ti₅O₁₂ (Figure 7a). [4c] Taking advantages including the high-spatial resolution as well as the high Li *K*-edge sensitivity to the local Li environment, the operando EELS results revealed the Li⁺ ion migration in the Li₄Ti₅O₁₂ from its initial tetrahedral 8a site to the polyhedral site as an intermediate and to the final octahedral 16c site in the Li₇Ti₅O₁₂, which was responsible for the fast charge behavior. Gao et al. employed EELS to investigate the chemical environmental changes for Li and Mn to better understand the phase transition mechanism of the spinel LiMn₂O₄ (Figure 7b). [66] The cation migration and anion shift, that is, Li_{tetrahedral} \rightarrow Li_{octahedral}, Mn_{octahedral} \rightarrow Mn_{tetrahedral} \rightarrow Mn_{octahedral}, and O_{low symmetric site} \rightarrow O_{high symmetric site}, induced the phase transition from the spinel

16163028, 2022, 1, Downloaded from https

onlinelibrary.wiley.com/doi/10.1002/adfm.202107190 by University Town Of Shenzhen, Wiley Online Library on [24/11/2025]. See the Terms and Conditions (https://onlinelibrary.wiley

and-conditions) on Wiley Online Library for rules of use; OA articles are governed by the applicable Creative Commons

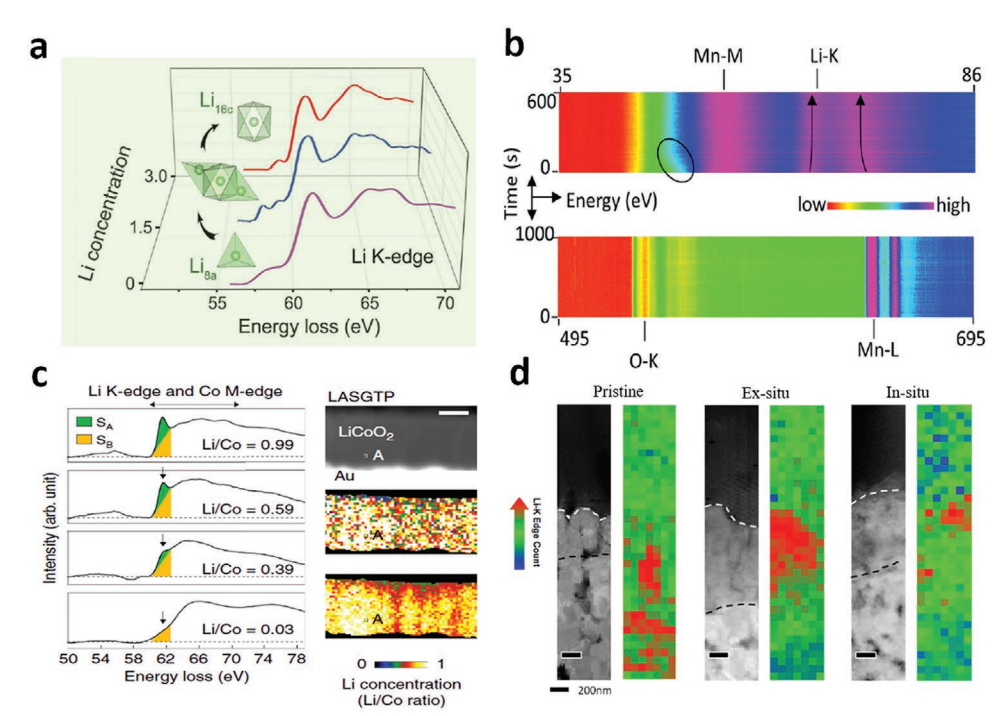


Figure 7. Monitoring of the dynamic Li⁺ migration and distributions. a) Real-time probing of Li⁺ transport in Li₄Ti₅O₁₂ during discharge and charge using the operando Li-EELS. Reproduced with permission. [4c] Copyright 2020, American Association for the Advancement of Science. b) 2D EELS maps showing the chemical evolution of Mn-M, Li-K, O-K, and Mn-L edges in LiMn₂O₄. Reproduced with permission. [66] Copyright 2017, American Chemical Society. c) Li K-edge EELS and Li concentration mapping of Li_XCoO₂. Reproduced with permission. [4b] Copyright 2020, Nature Publishing Group. d) STEM image and the Li K-edge concentration mapping of the all-solid-state LiCoO₂/LiPON/Li nanobattery. Reproduced with permission. [18b] Copyright 2016, American Chemical Society.

to the rock-salt while keeping the oxygen sub-lattice framework virtually unchanged.

The advanced MEMS-type electrochemical solid-state open cell has facilitated the direct observation of the distribution and the electronic states of Li in both the electrodes and solid electrolytes. By using operando EELS, Nomura et al. achieved the dynamic imaging of the Li in the LiCoO2/Li-Al-Ge(Ti)-Si-P-O/Li solid-state battery (Figure 7c). [4b] The Li concentration mapping and corresponding Li/Co ratio results indicated that the Li+ ions migrated not only along the vertical but also the parallel direction to the electrode/solid-electrolyte interface, causing the Li concentration to vary spatially at the nanoscale during the electrochemical reactions. Wang et al. used EELS to visualize the real-time interfacial phenomena related to the Li⁺ transport in the all-solid-state LiCoO₂/LiPON/Li battery (Figure 7d).^[18b] According to their findings, the LiCoO2/LiPON interfacial impedance was induced by the chemical changes instead of the space charge effects. The Li metal deposition/stripping in a mixed ionic-electronic conducting solid electrolyte was recently observed by the in situ TEM and further validated by the EELS.^[67] Similarly, the Li electrodeposition dynamics in the liquid aprotic electrolyte was also visualized via the in situ TEM, which was later confirmed by the EELS.[68]

5.4. Interfacial Behaviors

When the electrodes react with the electrolytes at the interfacial regions, the electrode/electrolyte interphases are

formed, including the SEI for the anodes and the CEI for the cathodes. [1c,3b] The instability of these interphases has been widely known as one of the crucial reasons for the battery capacity loss. [1c,69] Therefore, the electrode/electrolyte interphase observation is highly helpful in understanding the interfacial phenomena. And thanks to the development of the electrochemical cells for TEM, the in situ monitoring of the interphase formation/evolution is now possible. Furthermore, the cryo-EELS even allows the composition determination of some instable SEI and CEI films.

Because of the limited spatial resolution and the influence from the electrolyte in the electrochemical liquid close cell, in situ TEM/EELS observation of the SEI/CEI in the batteries using the commercial liquid electrolyte is currently almost impossible. Ex situ EELS is then applied to examine the SEI composition on different electrode materials, such as graphite, [70] Si, [71] hard carbon, [72] FeF2, [73] etc. To reduce the electron beam damage, Boniface et al. utilized the low-loss EELS (< 50 eV) to analyze the SEI evolution on the Si anode (Figure 8a). [74] The different plasmon peaks attributed to the SEI components (e.g., LiF, Li₂O, carbonates, Si, Li-Si alloy, carbon black, etc.) make it possible to observe the SEI evolution during charge-discharge if a sufficient SNR can be attained. They discovered that the SEI at the particle scale was extremely heterogeneous and evolutional with prolonged cycling, owing to the SEI accumulation and the transition from the Li-rich carbonate-like compounds to the Li-lean ones.

Since the thermal damage and the knock-on effect from the incident electrons in TEM can be effectively mitigated using

www.afm-iournal.de

16163028, 2022, 1, Downloaded from https

elibrary.wiley.com/doi/10.1002/adfm.202107190 by University Town Of Shenzhen, Wiley Online Library on [24/11/2025]. See the Terms and Conditions (https://onlinelibrary.wiley.

-and-conditions) on Wiley Online Library for rules of use; OA articles are governed by the applicable Creative Commons

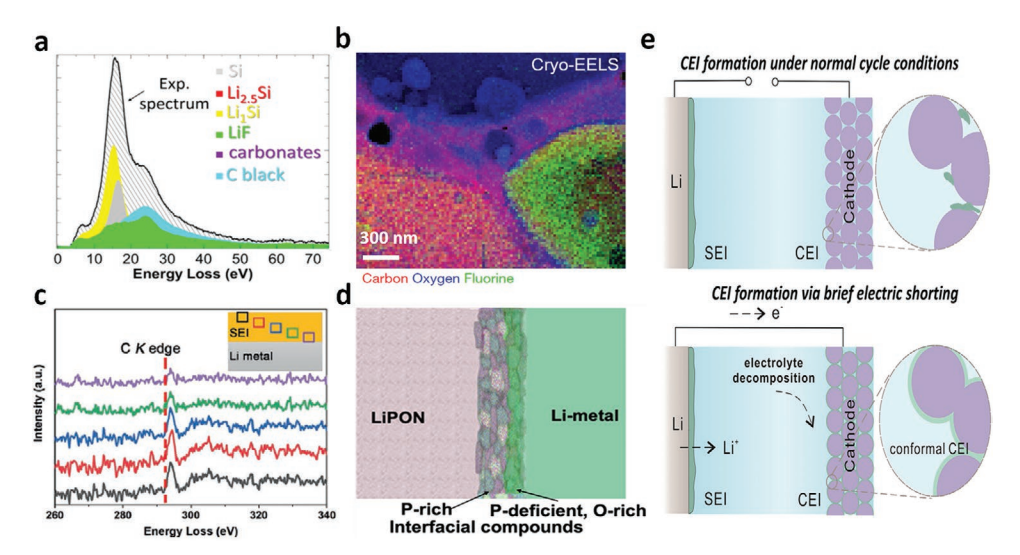


Figure 8. Electrode/electrolyte interphase observations. a) EELS spectrum of possible species in the lithiated Si anode. Reproduced with permission. [74] Copyright 2016, American Chemical Society. b) Cryo-EELS elemental mapping of SEI on the Li metal anode. Reproduced with permission. [4f] Copyright 2018, Nature Publishing Group. c) The C K-edge EELS spectrum acquired from the Li metal to the SEI surface in the EC/DEC electrolyte. Reproduced with permission. [82] Copyright 2021, Wiley-VCH. d) Schematic representation of the interphase formation between the Li metal and the solid LiPON electrolyte. Reproduced with permission. [83] Copyright 2021, American Chemical Society. e) Schematic of the CEI formation under different conditions revealed by cryo-EELS. Reproduced with permission. [80] Copyright 2021, Elsevier.

liquid nitrogen, [75] the invention of the cryo-EELS has opened a new door to analyzing the beam-sensitive components in the electrode/electrolyte interphases. So far, the cryo-EELS has been successfully employed to study the SEIs on the Li,[76] Sn,^[77] and Si anodes,^[78] as well as the CEIs on the spinel^[79] and the Ni-rich layered cathodes, [80] etc. For instance, Zachman et al. adopted the cryo-EELS to investigate the compositional elements of the Li dendrites as well as their interphase layers in the Li-metal batteries using the liquid LiPF₆/ethylene carbonate (EC)-based organic mixture electrolyte (Figure 8b).[4f] From the Li and H K-edge mapping, they identified two dendrite types on the Li anode surface: type-I was the partially oxidized Li metal while type-II was the homogenous lithium hydride (LiH). And according to the C, O, and F K-edge mapping, the oxygenrich SEI layer was exclusively detected in the type-I dendrite, while the fluorine-rich structures were always found in both the dendrite types. Similar experiments were also conducted by Cui and co-workers,[81] who proposed that the LiF could not be dominant in the Li anode passivation nor did it affect the Li+ ion migration through the compact SEI film. They also used cryo-TEM/EELS to explore the influence of the fluoroethylene carbonate (FEC) additive on the SEI, [76] and found that the multilayer SEI was formed on the Li anode in the FEC-containing electrolyte, rather than the mosaic SEI in the EC/diethyl carbonate (DEC) electrolyte. Gu and co-workers employed the cryo-TEM/EELS to study the SEI on the Li anode cycled in the EC/DEC electrolyte as well as the effect of the sulfur-containing additives (Figure 8c). [82] The TEM images, EELS mapping (Li, O, C, S), and the S and C K-edge spectra from the Li metal to the SEI surface were employed to determine the distribution of the Li_2O , Li_2CO_3 , and Li_2SO_4 compounds. The results showed that the Li₂CO₃ was continuously distributed in the outer SEI and reacted with the electrolyte to generated gas, leading to the dynamically evolving porous SEI. The sulfur-containing

additives caused the SEI to preferentially form the Li_2SO_4 and the over-lithiated lithium sulfates and lithium oxides, which encapsulated Li_2CO_3 in the middle, limited the SEI thickening, thus tenfold extended the battery life.

The CEI composition on the cathodes has been in controversy for a long time, due to its much lesser quantity when compared with the SEI on the anodes.[1c] Cui and co-workers adopted the cryo-EELS/TEM to study the CEI on the Ni-rich layered cathode cycled in the EC/DEC electrolyte (Figure 8e).[80] They found that under normal operating conditions, no intimate coating existed at the single-particle level. However, after brief external electrical shorting, the solid-electrolyte interphase, which normally occurred on the anodes, may develop on the cathodes and be in situ electrochemically converted into the conformal and stable CEI. The cryo-EELS results of the conformal CEI (mapping and fine structures of C K-edge, O K-edge, and Mn L-edge) indicated the organic polymeric composition of the alkyl carbonates, and the absence of the fluorine peak demonstrated that LiF was not a CEI component. In addition, the missing Mn signal also indicated the negligible TM loss during forming the CEI, which uniformly coated the whole electrode. Cryo-EELS was also used to determine the CEI composition on the high-voltage spinel LiNi_{0.5}Mn_{1.5}O₄ cathode cycled in the novel carbonate-free sulfone-based electrolyte.^[79]

The development of the MEMS-type electrochemical solid-state open cells has enabled the real-time observations of the electrode/electrolyte interphases. Wang et al. investigated the nanoscale interfacial phenomena in a LiCoO₂/LiPON/Si (LiPON: lithium phosphorus oxynitride) nanobattery by in situ EELS. [18b] Based on the STEM images and the Li K-edge concentration mapping, an unanticipated disordered interfacial layer existing between the LiCoO₂ cathode and the LiPON electrolyte was found inherent without cycling. And upon charging, the in situ EELS (Li, O, Co K-edge) demonstrated that this interfacial

16163028, 2022, 1, Downloaded from https://advanced.onlinelibrary.wiley.com/doi/10.1002/adfm.202107190 by University Town Of Shenzhen, Wiley Online Library on [24/11/2025]. See the Terms

) on Wiley Online Library for rules of use; OA articles are governed by the applicable Creative Commons

layer developed into the highly oxidized Co-ion species together with the lithium oxide and lithium peroxide. Hood et al. observed the dynamic evolvement of the LiPON-Li interface during the contact and biasing by in situ EELS/TEM. [83] The K-edge EELS mapping of the Li, P, and O elements and the fine structures regarding the electrode and the interface indicated the formation of a thin interface layer (\approx 60 nm) at the LiPON-Li interface during the contact, which comprised two conductive compounds (P-rich and P-deficient/O-rich) that ensured the interfacial electrochemical stability while also acting as a valid passivation layer (Figure 8d). [83] Several similar EELS characterizations on the interfacial structure of the all-solid-state batteries (i.e., LiCoO₂/Li-Al-Ge-P/Li, etc.) have also been reported. [5a,84]

5.5. Thermal Stability

The thermal stability of the battery materials and their intermediate states during the electrochemical cycling is critical for the safe operation of batteries since they can cause the thermal abuse and even fire. [85] When an in situ heating holder and EELS are combined, a one-of-a-kind method can be created to observe the thermal-induced changes in the nanoscale structures and the electron states of the battery materials (e.g., LiCoO_2 , [4e] Ni-rich layered oxides, [86] Na_xCoO_2 , [87] etc.). Upon heating, the thermal-induced phase transition always happens in various battery materials, which can be efficiently tracked by the helpful EELS to explore the related influencing factors.

Jo et al. compared the thermal stability of the delithiated Nirich layered oxides with different Al contents using the in situ TEM and EELS. [86] By analyzing the changes in the ΔE ($E_{\rm main}-E_{\rm pre-edge}$) of the O K-edge and the Ni and Co $L_{2,3}$ -edges from the ${\rm Li}_x{\rm Ni}_{0.835}{\rm Co}_{0.15}{\rm Al}_{0.015}{\rm O}_2$ (NCA83) and the ${\rm Li}_x{\rm Ni}_{0.8}{\rm Co}_{0.15}{\rm Al}_{0.05}{\rm O}_2$ (NCA80) cathodes, the role of Al in the Ni-rich layered cathodes was elucidated (**Figure 9**a,b). The layered NCA83 transformed to the rock-salt phase earlier with worse thermal stability than NCA80, indicating that Al could suppress the formation of the completely charged domains like the CoO₂-type O1 phase. The suppression

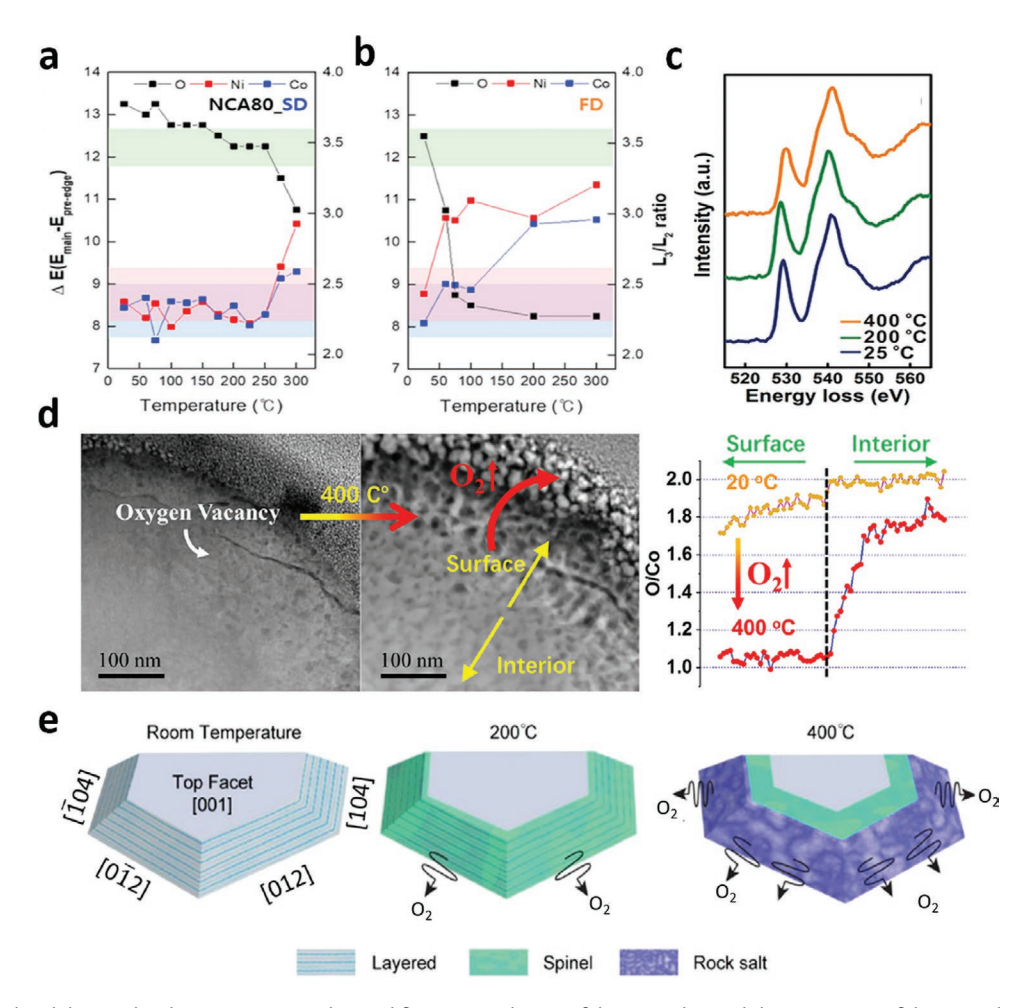


Figure 9. Thermal stability studies by in situ EELS. a,b) Modifications in the ΔE of the O K-edge and the L_3/L_2 ratio of the Ni and Co $L_{2,3}$ edges in the NCA80 (representative slow degrading (SD) and fast degrading (FD) particles). Reproduced with permission.^[86] Copyright 2020, Elsevier. c) EELS spectra of the O K-edge in LiNi_{0.8}Mn_{0.1}Co_{0.1}O₂ during heating. Reproduced with permission.^[89] Copyright 2015, American Chemical Society. d) TEM images with corresponding O/Co ratio derived from the quantitative EELS showing the oxygen release in the Li_xCoO₂. Reproduced with permission.^[90] Copyright 2020, American Chemical Society. e) Scheme showing the facet-dependent thermal instability of the LiCoO₂. Reproduced with permission.^[4e] Copyright 2017, American Chemical Society.

www.afm-journal.de

1616908, 2022, 1, Downloaded from https://advanced.onlinelibrary.wiley.com/doi/10.1002/affm.022107190 by University Town Of Shenzhen, Wiley Online Library on [247112025]. See the Terms and Conditions (https://onlinelibrary.wiley.com/rems-and-conditions) on Wiley Online Library for rules of use; OA acriles are governed by the applicable Cerative Commons I

effect thus inhibited the TMs reduction, particularly Co, which improved the thermal stability of the Ni-rich layered cathodes. By TEM and EELS. Pokle et al. observed a similar layered to rocksalt phase transformation in the Ni-rich Li(Ni_{0.85}Co_{0.15}Mn_{0.05})O₂ cathode. [88] The results suggested that such a phase transition preferred to occur at the internal interface, thus raising the intragrain heterogeneity. Hwang et al. explored the TM composition effects on the local thermal stability of the charged Li_xNi_vMn_zCo_{1-v-z}O₂ cathodes (y, z = 0.8, 0.1; 0.6, 0.2; 0.4, 0.3). The Ni-richest material (Li_xNi_{0.8}Mn_{0.1}Co_{0.1}O₂) instead of those with the other compositions was the most thermally unstable even at significantly low temperatures, as evidenced by the alterations in both the electronic structures and the phase transition onset at the temperatures as low as 100 °C. EELS indicated that these changes in the Li_xNi_{0.8}Mn_{0.1}Co_{0.1}O₂ material were driven by the Ni ions' thermal reduction, which was further deteriorated by the existence of the additional redox that occurred at 4.2 V (Figure 9c).

For the widely used layered oxide cathodes, the intrinsic mechanism of the thermal-induced phase transition is intriguing. As a nanoscale probe sensitive to the chemical environment of the cathode atoms (Li, Ni, Mn, O, etc.) and related defects, EELS has been applied to explore the origin of the thermal-induced phase transition. For instance, Sun et al. used the in situ EELS and TEM imaging to evaluate the oxygen release during heating the Li_xCoO₂ cathode after the high-voltage (4.6 V) cycling (Figure 9d). [90] From the EELS line scan, the O/Co ratio at the surface was lower than that in the bulk, suggesting the continuous oxygen loss near the surface region. Furthermore, they found that such thermal degradation was proceeded through the oxygen vacancies and facilitated by the cation migration and reduction. Because the kinetic degradation aided by the vacancies was a short-range process, they proposed that reducing the surface fraction would be a highly effective mitigating strategy.^[90] Sharifi-Asl et al. reported the similar oxygen release during the thermal degradation (phase transformation) of a chemically delithiated Li_xCoO₂ (Figure 9e),[4e] which was strongly dependent on the facet orientation. Combining the STEM images as well as the O K-edge and Co $L_{2,3}$ -edge evolution during the heating treatment, they found that the oxygen release) occurred on the particle surface of the chemically delithiated Li_xCoO_2 (x = 0.45, 0.7). They further associated this local oxygen evolution with the phase transitions, which spanned from the layered to the spinel and finally to the rock-salt structure when exposed to the elevated temperature.[4e] Yan et al. also reported the similar oxygen release and phase transition behaviors in the delithiated Ni-rich LiNi_{0.6}Mn_{0.2}Co_{0.2}O₂ cathode.^[91] They claimed that the thermal stress related to the electrochemical-induced phase heterogeneity and the internal pressure caused by the oxygen release were the major force driving the intragranular cracks, which resembled the "popcorn" fracture mechanism. The thermal stability of other electrode materials, like the P2-type Na_xCoO₂ and the graphene, has also been investigated by EELS.[87,92]

5.6. Others

Besides the above studies, EELS also has many other battery-related applications, e.g., regeneration of the battery

cathodes,^[93] changes in the electrodes after aging,^[26d] prelithiation of the electrodes,^[94] electrolyte degradation mechanism under the electron beam,^[95] etc. They all involve the elemental distribution and the electron state changes.

For example, Shi et al. combined the atomic-level TEM imaging and EELS to investigate the structure of a relithiated degraded LiNi_{0.5}Co_{0.2}Mn_{0.3}O₂ (NCM523) cathode.^[93] When the bulk Li K-edge EELS spectra of the degraded and the regenerated NCM523 samples were compared, a considerably larger Li content was found in the latter. In the O K-edge spectra, the pre-edge structure below 534 eV corresponded to the state transition of the TM 3d and the oxygen 2p orbitals. The intensity decrease in the pre-edge structure of the degraded NCM523 suggested the change in the bond covalency between the TM and the neighboring oxygen, which was caused by the generation of the Ni-O like rock-salt phase on the material surface. However, there was no discernible difference in the pre-edge structure from the surface to the bulk in the regenerated NCM523, manifesting the surface structure recovery. Nagpure et al. utilized EELS, TEM imaging, and theoretical calculations for investigating the effects of the LIB aging on the local electronic structure of the LiFePO₄ nanoparticles.^[26d] Both the experimental and calculated O K-edge and Fe L2,3-edge suggested the active Li loss from the LiFePO4 host in the aged battery, corresponding to the capacity loss. To achieve both the high capacity and stability, Sun et al. reported a Li₃N prelithiation additive in the layered oxide and the LiFePO₄ hybrid electrodes.^[96] They adopted EELS to confirm the dense surface passivation layer comprising the crystalline Li₂O and Li₂CO₃, which protected the active materials from the atmosphere and enabled the Li₃N particles to be stable under the ambient conditions. By employing the valence-band EELS characterization, Abellan et al. investigated the real-time degradation mechanism of several electrolytes (LiAsF₆/EC/DMC, LiAsF₆/DMC, LiAsF₆/ DMSO(dimethyl sulfoxide), LiTf(lithium triflate)/DMSO) under the electron beam.^[95] The main degradation products in these four electrolytes appeared to contain arsenic, which may be existing in the form of the AsF₃ or the completely reduced As⁰. These in situ (S)TEM-EELS results are comparable with the previous stability experiments conducted under the real-time battery operation, together with the decomposition products and mechanisms similar to the reported ones.

6. Conclusions and Perspectives

In summary, owing to the distinctive capabilities as well as the recently developed advanced measurement configurations, EELS has been successfully employed to study various important battery issues and made significant progress, such as the atomic-level element distribution and the electronic state determination of the electrodes, exploration of the intermediate states during cycling, in situ monitoring of the dynamic Li⁺ migration/distribution, instable SEI composition on the Li metal surface, interfacial phenomena of the all-solid-state battery, thermal stability of the electrode materials, etc.

However, in spite of these battery studies achieved by EELS, there are still some challenges and opportunities remained. 1) Development of the advanced configurations for EELS, e.g., in situ

16163028, 2022, 1, Downloaded from https://advanced.onlinelibrary.wiley.com/doi/10.1002/adfm.202107190 by University Town Of Shenzhen, Wiley Online Library on [24/11/2025]. See the Terms and Conditions (https://onlinelibrary.wiley

and-conditions) on Wiley Online Library for rules of use; OA articles are governed by the applicable Creative Commons

ADVANCED FUNCTIONAL MATERIALS

(e.g., electrochemical) cryo-holders, high-resolution liquid close cells, etc., still requires much effort and will further facilitate the battery studies. 2) Because the Li⁺ migration is usually difficult to be characterized by other conventional techniques, more attention should be devoted to employing the in situ EELS for revealing the in-depth Li⁺ migration in the electrode materials, including different types of cathodes and anodes for LIBs and other novel batteries (i.e., Li-S, Li-O2, etc.). 3) Although the EELS-based RDF analysis for the battery materials has received little attention in the past decade due to the low SNR, the newly developed highly sensitive detectors and cameras have opened up new opportunities of using EELS as an efficient tool for the nanoscale RDF analysis, especially for the amorphous phases and defects. Therefore, the combination of the RDF analysis and the in situ configurations is very promising. 4) Development in the ultrafast camera and highly sensitive detector also benefits the energy resolution of the plasmon peak and the operability of the 3D EELS tomography, which will further promote understanding the crystal and chemical structures of LIBs and other alkali-metal (i.e., Li, Na, K, etc.) batteries through the combination of 3D EELS with cryo-TEM.

Overall, it is believed that EELS will undoubtedly play a more powerful role in studying the next-generation battery due to its distinct capabilities, enabling the comprehensive understandings regarding the elemental types with their valence and concentration distributions, and the structure-related atom radial distribution in battery materials. Further utilization of the EELS technique in the battery studies may need to be focused on exploring the innovative in situ configurations and improving the energy and spatial resolution.

Acknowledgements

Z.-W.Y., W.Z., J.L. contributed equally to this work. This work was supported by the National Key R&D Program of China (No. 2020YFB0704500), Shenzhen Science and Technology Research Grants (No. JCYJ20200109140416788) and China Postdoctoral Science Foundation (No. 2020M680198). Z.W.Y. thanks Kai Wang (Karlsruhe Institute of Technology (KIT), Germany) for his significant comments on the logic and contents of this paper.

Conflict of Interest

The authors declare no conflict of interest.

Keywords

battery materials, chemical composition, electron energy loss spectroscopy, intermediate states, Li⁺ migration, scanning transmission electron microscopy, thermal stability, transmission electron microscopy

Received: July 24, 2021 Revised: September 7, 2021 Published online: September 24, 2021

[1] a) T. Liu, L. Lin, X. Bi, L. Tian, K. Yang, J. Liu, M. Li, Z. Chen, J. Lu, K. Amine, K. Xu, F. Pan, Nat. Nanotechnol. 2019, 14, 50; b) J. Li, C. Lin, M. Weng, Y. Qiu, P. Chen, K. Yang, W. Huang, Y. Hong, J. Li, M. Zhang, C. Dong, W. Zhao, Z. Xu, X. Wang, K. Xu, J. Sun, F. Pan,

- Nat. Nanotechnol. 2021, 16, 599; c) K. Xu, Chem. Rev. 2014, 114, 11503.
- [2] a) M. Gong, W. Zhou, M. J. Kenney, R. Kapusta, S. Cowley, Y. Wu, B. Lu, M. C. Lin, D. Y. Wang, J. Yang, B. J. Hwang, H. Dai, Angew. Chem., Int. Ed. Engl. 2015, 54, 11989; b) P. Nandi, E. Hoglund, X. Sang, R. R. Unocic, J. M. Howe, Microsc. Microanal. 2017, 23, 414; c) M. Ge, Y. Lu, P. Ercius, J. Rong, X. Fang, M. Mecklenburg, C. Zhou, Nano Lett. 2014, 14, 261.
- [3] a) J. Lu, T. Wu, K. Amine, Nat. Energy 2017, 2, 17011; b) A. M. Tripathi,
 W. N. Su, B. J. Hwang, Chem. Soc. Rev. 2018, 47, 736.
- [4] a) J. Y. Huang, L. Zhong, C. M. Wang, J. P. Sullivan, W. Xu, L. Q. Zhang, S. X. Mao, N. S. Hudak, X. H. Liu, A. Subramanian, H. Y. Fan, L. A. Qi, A. Kushima, J. Li, Science 2010, 330, 1515; b) Y. Nomura, K. Yamamoto, M. Fujii, T. Hirayama, E. Igaki, K. Saitoh, Nat. Commun. 2020, 11, 2824; c) W. Zhang, D. H. Seo, T. Chen, L. Wu, M. Topsakal, Y. Zhu, D. Lu, G. Ceder, F. Wang, Science 2020, 367, 1030; d) M. E. Holtz, Y. Yu, D. Gunceler, J. Gao, R. Sundararaman, K. A. Schwarz, T. A. Arias, H. D. Abruna, D. A. Muller, Nano Lett. 2014, 14, 1453; e) S. Sharifi-Asl, F. A. Soto, A. Nie, Y. Yuan, H. Asayesh-Ardakani, T. Foroozan, V. Yurkiv, B. Song, F. Mashayek, R. F. Klie, K. Amine, J. Lu, P. B. Balbuena, R. Shahbazian-Yassar, Nano Lett. 2017, 17, 2165; f) M. J. Zachman, Z. Tu, S. Choudhury, L. A. Archer, L. F. Kourkoutis, Nature 2018, 560, 345.
- [5] a) C. Zhang, Y. Feng, Z. Han, S. Gao, M. Wang, P. Wang, Adv. Mater. 2020, 32, 1903747; b) C. Zhang, K. L. Firestein, J. F. S. Fernando, D. Siriwardena, J. E. von Treifeldt, D. Golberg, Adv. Mater. 2020, 32, 1904094; c) T. Shang, Y. Wen, D. Xiao, L. Gu, Y.-S. Hu, H. Li, Adv. Energy Mater. 2017, 7, 1700709; d) F. Wu, N. Yao, Nano Energy 2015, 11, 196.
- [6] a) X. Liu, W. Yang, Z. Liu, Adv. Mater. 2014, 26, 7710; b) F. Lin, Y. Liu, X. Yu, L. Cheng, A. Singer, O. G. Shpyrko, H. L. Xin, N. Tamura, C. Tian, T. C. Weng, X. Q. Yang, Y. S. Meng, D. Nordlund, W. Yang, M. M. Doeff, Chem. Rev. 2017, 117, 13123.
- [7] a) Y. Wu, G. Li, J. P. Camden, Chem. Rev. 2018, 118, 2994;
 b) C. Cherqui, N. Thakkar, G. Li, J. P. Camden, D. J. Masiello, Annu. Rev. Phys. Chem. 2016, 67, 331.
- [8] S. M. Collins, P. A. Midgley, Ultramicroscopy 2017, 180, 133.
- [9] a) K. Yamamoto, Y. Iriyama, T. Hirayama, Microscopy 2017, 66, 50; b) O. L. Krivanek, N. Dellby, J. A. Hachtel, J. C. Idrobo, M. T. Hotz, B. Plotkin-Swing, N. J. Bacon, A. L. Bleloch, G. J. Corbin, M. V. Hoffman, C. E. Meyer, T. C. Lovejoy, Ultramicroscopy 2019, 202, 60
- [10] B. A. Carter, D. B. Williams, C. B. Carter, D. B. Williams, Transmission Electron Microscopy: A Textbook for Materials Science. Diffraction. II, Springer Science & Business Media, Berlin 1996.
- [11] H. T. Chung, D. A. Cullen, D. Higgins, B. T. Sneed, E. F. Holby, K. L. More, P. Zelenay, *Science* 2017, 357, 479.
- [12] J. Lim, Y. Li, D. H. Alsem, H. So, S. C. Lee, P. Bai, D. A. Cogswell, X. Liu, N. Jin, Y.-s. Yu, Science 2016, 353, 566.
- [13] R. F. Egerton, Electron Energy-Loss Spectroscopy in the Electron Microscope, Springer Science & Business Media, Berlin 2011.
- [14] X. Li, Z. Ren, M. Norouzi Banis, S. Deng, Y. Zhao, Q. Sun, C. Wang, X. Yang, W. Li, J. Liang, X. Li, Y. Sun, K. Adair, R. Li, Y. Hu, T.-K. Sham, H. Huang, L. Zhang, S. Lu, J. Luo, X. Sun, ACS Energy Lett. 2019, 4, 2480.
- [15] P. Torruella, R. Arenal, F. de la Pena, Z. Saghi, L. Yedra, A. Eljarrat, L. Lopez-Conesa, M. Estrader, A. Lopez-Ortega, G. Salazar-Alvarez, J. Nogues, C. Ducati, P. A. Midgley, F. Peiro, S. Estrade, *Nano Lett.* 2016, 16, 5068.
- [16] a) J. B. Souza Junior, G. R. Schleder, J. Bettini, I. C. Nogueira, A. Fazzio, E. R. Leite, *Matter* 2021, 4, 441; b) R. D. B. Evans, J. More, K. L. Doll, G. L. Glass, J. Appl. Phys. 2004, 96, 273; c) X. Mu, A. Mazilkin, C. Sprau, A. Colsmann, C. Kubel, *Microscopy* 2019, 68, 301.

16163028, 2022, 1, Downloaded from https://advanced.onlinelibrary.wiley.com/doi/10.1002/adfm.202107190 by University Town Of Shenzhen, Wiley Online Library on [24/11/2025]. See the Terms and Conditions (https://onlinelibrary.wiley

and-conditions) on Wiley Online Library for rules of use; OA articles are governed by the applicable Creative Commons

- [17] J. L. Hart, A. C. Lang, R. B. Cummings, I. MacLaren, M. L. Taheri, Microsc. Microanal. 2019, 25, 584.
- [18] a) Y. Liu, N. S. Hudak, D. L. Huber, S. J. Limmer, J. P. Sullivan, J. Y. Huang, Nano Lett. 2011, 11, 4188; b) Z. Wang, D. Santhanagopalan, W. Zhang, F. Wang, H. L. Xin, K. He, J. Li, N. Dudney, Y. S. Meng, Nano Lett. 2016, 16, 3760.
- [19] Y. Li, Y. Li, A. Pei, K. Yan, Y. Sun, C. L. Wu, L. M. Joubert, R. Chin, A. L. Koh, Y. Yu, J. Perrino, B. Butz, S. Chu, Y. Cui, *Science* 2017, 358, 506
- [20] N. Jian, P. Xue, D. Diao, Appl. Surf. Sci. 2019, 498, 143831.
- [21] J. Y. Huang, L. Zhong, C. M. Wang, J. P. Sullivan, W. Xu, L. Q. Zhang, S. X. Mao, N. S. Hudak, X. H. Liu, A. Subramanian, H. Fan, L. Qi, A. Kushima, J. Li, Science 2010, 330, 1515.
- [22] F. Wang, H. C. Yu, M. H. Chen, L. Wu, N. Pereira, K. Thornton, A. Van der Ven, Y. Zhu, G. G. Amatucci, J. Graetz, *Nat. Commun.* 2012, 3, 1201.
- [23] a) S.-Y. Lee, J. Shangguan, J. Alvarado, S. Betzler, S. J. Harris, M. M. Doeff, H. Zheng, *Energy Environ. Sci.* 2020, 13, 1832;
 b) Z. Zeng, W. I. Liang, H. G. Liao, H. L. Xin, Y. H. Chu, H. Zheng, *Nano Lett.* 2014, 14, 1745;
 c) Z. Zeng, P. Barai, S.-Y. Lee, J. Yang, X. Zhang, W. Zheng, Y.-S. Liu, K. C. Bustillo, P. Ercius, J. Guo, *Nano Energy* 2020, 72, 104721.
- [24] L. Yu, B. M. Hudak, A. Ullah, M. P. Thomas, C. C. Porter, A. Thisera, R. H. Pham, M. De Alwis Goonatilleke, B. S. Guiton, *Chem. Mater.* 2020, 32, 639.
- [25] a) Y. Liu, Z. Ju, B. Zhang, Y. Wang, J. Nai, T. Liu, X. Tao, Acc. Chem. Res. 2021, 54, 2088; b) X. Wang, Y. Li, Y. S. Meng, Joule 2018, 2, 2225
- [26] a) Y. M. Wang, S. Cheng, Q. M. Wei, E. Ma, T. G. Nieh, A. Hamza, Scr. Mater. 2004, 51, 1023; b) P. Agrawal, J. Guo, P. Yu, C. Hébert, D. Passerone, R. Erni, M. D. Rossell, Phys. Rev. B 2016, 94, 104101; c) V. J. Keast, Mater. Charact. 2012, 73, 1; d) S. C. Nagpure, S. S. Babu, B. Bhushan, A. Kumar, R. Mishra, W. Windl, L. Kovarik, M. Mills, Acta Mater. 2011, 59, 6917.
- [27] F. Lin, D. Nordlund, Y. Li, M. K. Quan, L. Cheng, T.-C. Weng, Y. Liu, H. L. Xin, M. M. Doeff, Nat. Energy 2016, 1, 15004.
- [28] J. Gázquez, G. Sánchez-Santolino, N. Biškup, M. A. Roldán, M. Cabero, S. J. Pennycook, M. Varela, *Mater. Sci. Semicond. Process.* 2017. 65. 49.
- [29] S. Hwang, X. Chen, G. Zhou, D. Su, Adv. Energy Mater. 2019, 10, 1902105
- [30] a) I. S. Cole, D. Marney, Corros. Sci. 2012, 56, 5; b) G. Wang,
 L. Zhang, J. Zhang, Chem. Soc. Rev. 2012, 41, 797; c) D. Higgins,
 P. Zamani, A. P. Yu, Z. W. Chen, Energy Environ. Sci. 2016, 9, 357;
 d) R. Manivannan, S. N. Victoria, Sol. Energy 2018, 173, 1144;
 e) N. Loukil, M. Feki, J. Electrochem. Soc. 2020, 167, 022503.
- [31] Y. Xiao, Y. F. Zhu, H. R. Yao, P. F. Wang, X. D. Zhang, H. Li, X. Yang, L. Gu, Y. C. Li, T. Wang, Y. X. Yin, X. D. Guo, B. H. Zhong, Y. G. Guo, Adv. Energy Mater. 2019, 9, 1803978.
- [32] a) L. Wang, P. E. Vullum, K. Asheim, X. Wang, A. M. Svensson, F. Vullum-Bruer, Nano Energy 2018, 48, 227; b) Q. Tan, X. Li, B. Zhang, X. Chen, Y. Tian, H. Wan, L. Zhang, L. Miao, C. Wang, Y. Gan, J. Jiang, Y. Wang, H. Wang, Adv. Energy Mater. 2020, 10, 2001050; c) Y. Liang, C. Luo, F. Wang, S. Hou, S. C. Liou, T. Qing, Q. Li, J. Zheng, C. Cui, C. Wang, Adv. Energy Mater. 2018, 9, 1802986; d) Y. Chen, X. Li, K. Park, W. Lu, C. Wang, W. Xue, F. Yang, J. Zhou, L. Suo, T. Lin, H. Huang, J. Li, J. B. Goodenough, Chem 2017, 3, 152; e) C. Li, L. Gu, S. Tsukimoto, P. A. van Aken, J. Maier, Adv. Mater. 2010, 22, 3650.
- [33] J. Song, M. L. Gordin, T. Xu, S. Chen, Z. Yu, H. Sohn, J. Lu, Y. Ren, Y. Duan, D. Wang, Angew. Chem., Int. Ed. Engl. 2015, 54, 4325.
- [34] L. Yang, L. Shi, D. Wang, Y. Lv, D. Cao, Nano Energy 2018, 50, 691.
- [35] X. Liu, Y. Chen, Z. D. Hood, C. Ma, S. Yu, A. Sharafi, H. Wang, K. An, J. Sakamoto, D. J. Siegel, Y. Cheng, N. H. Jalarvo, M. Chi, Energy Environ. Sci. 2019, 12, 945.

- [36] R. J. Nicholls, A. T. Murdock, J. Tsang, J. Britton, T. J. Pennycook, A. Koos, P. D. Nellist, N. Grobert, J. R. Yates, ACS Nano 2013, 7, 7145.
- [37] J. Lee, W. Zhou, J. C. Idrobo, S. J. Pennycook, S. T. Pantelides, *Phys. Rev. Lett.* **2011**, *107*, 085507.
- [38] X. Guo, M. Wang, X. Huang, P. Zhao, X. Liu, R. Che, J. Mater. Chem. A 2013. 1, 8775.
- [39] S. W. Oh, S. T. Myung, S. M. Oh, K. H. Oh, K. Amine, B. Scrosati, Y. K. Sun, Adv. Mater. 2010, 22, 4842.
- [40] J. Kim, J. Lee, H. Ma, H. Y. Jeong, H. Cha, H. Lee, Y. Yoo, M. Park, J. Cho, Adv. Mater. 2018, 30, 1704309.
- [41] W. Li, Y. Tang, W. Kang, Z. Zhang, X. Yang, Y. Zhu, W. Zhang, C. S. Lee, Small 2015, 11, 1345.
- [42] K. Wang, Z.-G. Wu, G. Melinte, Z.-G. Yang, A. Sarkar, W. Hua, X. Mu, Z.-W. Yin, J.-T. Li, X.-D. Guo, B.-H. Zhong, C. Kübel, J. Mater. Chem. A 2021, 9, 13151.
- [43] D. Chao, C. Ye, F. Xie, W. Zhou, Q. Zhang, Q. Gu, K. Davey, L. Gu, S. Z. Qiao, Adv. Mater. 2020, 32, 2001894.
- [44] J. Ding, H. Zhang, H. Zhou, J. Feng, X. Zheng, C. Zhong, E. Paek, W. Hu, D. Mitlin, Adv. Mater. 2019, 31, 1900429.
- [45] a) L. C. Loaiza, L. Monconduit, V. Seznec, Small 2020, 16, 1905260;
 b) Z. Lyu, Y. Zhou, W. Dai, X. Cui, M. Lai, L. Wang, F. Huo, W. Huang, Z. Hu, W. Chen, Chem. Soc. Rev. 2017, 46, 6046; c) Y. Yan, C. Cheng, L. Zhang, Y. Li, J. Lu, Adv. Energy Mater. 2019, 9, 1900148.
- [46] a) M. E. Schuster, D. Teschner, J. Popovic, N. Ohmer, F. Girgsdies, J. Tornow, M. G. Willinger, D. Samuelis, M.-M. Titirici, J. Maier, R. Schlögl, *Chem. Mater.* 2014, 26, 1040; b) Z. Yang, Z. Zhu, J. Ma, D. Xiao, X. Kui, Y. Yao, R. Yu, X. Wei, L. Gu, Y.-S. Hu, H. Li, X. Zhang, *Adv. Energy Mater.* 2016, 6, 1600806; c) J. Lee, D.-H. Seo, M. Balasubramanian, N. Twu, X. Li, G. Ceder, *Energy Environ. Sci.* 2015, 8, 3255.
- [47] S. Zhang, G. Wang, J. Jin, L. Zhang, Z. Wen, J. Yang, Nano Energy 2017, 36, 186.
- [48] L. Laffont, C. Delacourt, P. Gibot, M. Y. Wu, P. Kooyman, C. Masquelier, J. M. Tarascon, Chem. Mater. 2006, 18, 5520.
- [49] J. Li, S. Hwang, F. Guo, S. Li, Z. Chen, R. Kou, K. Sun, C. J. Sun, H. Gan, A. Yu, E. A. Stach, H. Zhou, D. Su, *Nat. Commun.* 2019, 10, 2224.
- [50] Q. Su, J. Zhang, Y. Wu, G. Du, Nano Energy 2014, 9, 264.
- [51] X. Lv, J. Deng, B. Wang, J. Zhong, T.-K. Sham, X. Sun, X. Sun, Chem. Mater. 2017, 29, 3499.
- [52] J. Kikkawa, S. Terada, A. Gunji, T. Nagai, K. Kurashima, K. Kimoto, J. Phys. Chem. C 2015, 119, 15823.
- [53] a) A. Boulineau, L. Simonin, J. F. Colin, C. Bourbon, S. Patoux, Nano Lett. 2013, 13, 3857; b) P. Yan, J. Zheng, Z. K. Tang, A. Devaraj, G. Chen, K. Amine, J. G. Zhang, L. M. Liu, C. Wang, Nat. Nanotechnol. 2019, 14, 602.
- [54] Y. Wen, X. Chen, X. Lu, L. Gu, J. Energy Chem. 2018, 27, 1397.
- [55] a) B. D. Adams, C. Radtke, R. Black, M. L. Trudeau, K. Zaghib, L. F. Nazar, Energy Environ. Sci. 2013, 6, 1772; b) H. G. Jung, J. Hassoun, J. B. Park, Y. K. Sun, B. Scrosati, Nat. Chem. 2012, 4, 579.
- [56] B. Ge, Y. Sun, J. Guo, X. Yan, C. Fernandez, Q. Peng, Small 2019, 15, 1902220.
- [57] X. Hu, J. Sun, Z. Li, Q. Zhao, C. Chen, J. Chen, Angew. Chem., Int. Ed. Engl. 2016, 55, 6482.
- [58] Y. Liu, R. Wang, Y. Lyu, H. Li, L. Chen, Energy Environ. Sci. 2014, 7, 677.
- [59] Q. Liu, L. Geng, T. Yang, Y. Tang, P. Jia, Y. Li, H. Li, T. Shen, L. Zhang, J. Huang, Energy Storage Mater. 2019, 19, 48.
- [60] B. Ge, Y. Wang, Y. Sun, Y. Li, J. Huang, Q. Peng, Energy Storage Mater. 2019, 23, 733.
- [61] A. Manthiram, ACS Cent. Sci. 2017, 3, 1063.
- [62] a) V. Mauchamp, F. Boucher, G. Ouvrard, P. Moreau, *Phys. Rev. B* 2006, *B74*, 115106; b) J. Kikkawa, S. Terada, A. Gunji, M. Haruta,



www.afm-journal.de

16163028, 2022, 1, Downloaded from https

onlinelibrary.wiley.com/doi/10.1002/adfm.202107190 by University Town Of Shenzhen, Wiley Online Library on [24/11/2025]. See the Terms

and-conditions) on Wiley Online Library for rules

of use; OA

are

governed by the applicable Creative Commons



- T. Nagai, K. Kurashima, K. Kimoto, *Appl. Phys. Lett.* **2014**, *104*, 114105.
- [63] A. Hightower, C. C. Ahn, B. Fultz, P. Rez, Appl. Phys. Lett. 2000, 77, 238.
- [64] F. Wang, J. Graetz, M. S. Moreno, C. Ma, L. Wu, V. Volkov, Y. Zhu, ACS Nano 2011, 5, 1190.
- [65] L. Gu, C. Zhu, H. Li, Y. Yu, C. Li, S. Tsukimoto, J. Maier, Y. Ikuhara, J. Am. Chem. Soc. 2011, 133, 4661.
- [66] P. Gao, R. Ishikawa, E. Tochigi, A. Kumamoto, N. Shibata, Y. Ikuhara, Chem. Mater. 2017, 29, 1006.
- [67] Y. Chen, Z. Wang, X. Li, X. Yao, C. Wang, Y. Li, W. Xue, D. Yu, S. Y. Kim, F. Yang, A. Kushima, G. Zhang, H. Huang, N. Wu, Y. W. Mai, J. B. Goodenough, J. Li, *Nature* 2020, 578, 251.
- [68] A. J. Leenheer, K. L. Jungjohann, K. R. Zavadil, J. P. Sullivan, C. T. Harris, ACS Nano 2015, 9, 4379.
- [69] D. G. Kwabi, Y. Ji, M. J. Aziz, Chem. Rev. 2020, 120, 6467.
- [70] Y. Lei, D. Han, J. Dong, L. Qin, X. Li, D. Zhai, B. Li, Y. Wu, F. Kang, Energy Storage Mater. 2020, 24, 319.
- [71] a) C. Stetson, T. Yoon, J. Coyle, W. Nemeth, M. Young, A. Norman, S. Pylypenko, C. Ban, C.-S. Jiang, M. Al-Jassim, A. Burrell, *Nano Energy* 2019, 55, 477; b) Y. Kamikawa, K. Amezawa, K. Terada, *J. Phys. Chem. C* 2021, 125, 3890.
- [72] F. A. Soto, P. Yan, M. H. Engelhard, A. Marzouk, C. Wang, G. Xu, Z. Chen, K. Amine, J. Liu, V. L. Sprenkle, F. El-Mellouhi, P. B. Balbuena, X. Li, Adv. Mater. 2017, 29, 1606860.
- [73] M. Sina, R. Thorpe, S. Rangan, N. Pereira, R. A. Bartynski, G. G. Amatucci, F. Cosandey, J. Phys. Chem. C 2015, 119, 9762.
- [74] M. Boniface, L. Quazuguel, J. Danet, D. Guyomard, P. Moreau, P. Bayle-Guillemaud, Nano Lett. 2016, 16, 7381.
- [75] a) C. J. Russo, R. F. Egerton, MRS Bull. 2019, 44, 935; b) D. A. M. De Winter, C. Hsieh, M. Marko, M. F. Hayles, J. Microsc. 2020, 281, 125.
- [76] Y. Li, W. Huang, Y. Li, A. Pei, D. T. Boyle, Y. Cui, Joule 2018, 2, 2167.
- [77] J. Huang, X. Guo, X. Du, X. Lin, J.-Q. Huang, H. Tan, Y. Zhu, B. Zhang, Energy Environ. Sci. 2019, 12, 1550.
- [78] W. Huang, J. Wang, M. R. Braun, Z. Zhang, Y. Li, D. T. Boyle, P. C. McIntyre, Y. Cui, Matter 2019, 1, 1232.
- [79] J. Alvarado, M. A. Schroeder, M. Zhang, O. Borodin, E. Gobrogge, M. Olguin, M. S. Ding, M. Gobet, S. Greenbaum, Y. S. Meng, K. Xu, Mater. Today 2018. 21, 341.
- [80] Z. Zhang, J. Yang, W. Huang, H. Wang, W. Zhou, Y. Li, Y. Li, J. Xu, W. Huang, W. Chiu, Y. Cui, *Matter* 2021, 4, 302.

- [81] W. Huang, H. Wang, D. T. Boyle, Y. Li, Y. Cui, ACS Energy Lett. 2020, 5, 1128.
- [82] B. Han, Z. Zhang, Y. Zou, K. Xu, G. Xu, H. Wang, H. Meng, Y. Deng, J. Li, M. Gu, Adv. Mater. 2021, 33, 2100404.
- [83] Z. D. Hood, X. Chen, R. L. Sacci, X. Liu, G. M. Veith, Y. Mo, J. Niu, N. J. Dudney, M. Chi, Nano Lett. 2021, 21, 151.
- [84] Y. Nomura, K. Yamamoto, T. Hirayama, M. Ohkawa, E. Igaki, N. Hojo, K. Saitoh, Nano Lett. 2018, 18, 5892.
- [85] a) X. Feng, M. Ouyang, X. Liu, L. Lu, Y. Xia, X. He, Energy Storage Mater. 2018, 10, 246; b) H. Liu, Z. Wei, W. He, J. Zhao, Energy Convers. Manage. 2017, 150, 304; c) X. N. Feng, S. Q. Zheng, D. S. Ren, X. M. He, L. Wang, H. Cui, X. Liu, C. Y. Jin, F. S. Zhang, C. S. Xu, H. J. Hsu, S. Gao, T. Y. Chen, Y. L. Li, T. Z. Wang, H. Wang, M. G. Li, M. G. Ouyang, Appl. Energy 2019, 246, 53.
- [86] E. Jo, J.-H. Park, J. Park, J. Hwang, K. Y. Chung, K.-W. Nam, S. M. Kim, W. Chang, Nano Energy 2020, 78, 105367.
- [87] S. Hwang, Y. Lee, E. Jo, K. Y. Chung, W. Choi, S. M. Kim, W. Chang, ACS Appl. Mater. Interfaces 2017, 9, 18883.
- [88] A. Pokle, S. Ahmed, S. Schweidler, M. Bianchini, T. Brezesinski, A. Beyer, J. Janek, K. Volz, ACS Appl. Mater. Interfaces 2020, 12, 57047.
- [89] S. Hwang, S. M. Kim, S.-M. Bak, S. Y. Kim, B.-W. Cho, K. Y. Chung, J. Y. Lee, E. A. Stach, W. Chang, *Chem. Mater.* 2015, 27, 3927.
- [90] C. Sun, X. Liao, F. Xia, Y. Zhao, L. Zhang, S. Mu, S. Shi, Y. Li, H. Peng, G. Van Tendeloo, K. Zhao, J. Wu, ACS Nano 2020, 14, 6181
- [91] P. Yan, J. Zheng, T. Chen, L. Luo, Y. Jiang, K. Wang, M. Sui, J. G. Zhang, S. Zhang, C. Wang, Nat. Commun. 2018, 9, 2437
- [92] a) M. Pelaez-Fernandez, A. Bermejo, A. M. Benito, W. K. Maser, R. Arenal, *Carbon* 2021, 178, 477; b) J. H. Warner, Y. C. Lin, K. He, M. Koshino, K. Suenaga, *Nano Lett.* 2014, 14, 6155.
- [93] Y. Shi, M. Zhang, Y. S. Meng, Z. Chen, Adv. Energy Mater. 2019, 9, 1900454
- [94] J. Zhao, Z. Lu, N. Liu, H. W. Lee, M. T. McDowell, Y. Cui, Nat. Commun. 2014, 5, 5088.
- [95] P. Abellan, B. L. Mehdi, L. R. Parent, M. Gu, C. Park, W. Xu, Y. Zhang, I. Arslan, J. G. Zhang, C. M. Wang, J. E. Evans, N. D. Browning, Nano Lett. 2014, 14, 1293.
- [96] Y. Sun, Y. Li, J. Sun, Y. Li, A. Pei, Y. Cui, Energy Storage Mater. 2017, 6 119



Zu-Wei Yin received his Ph.D. degree from Xiamen University in 2019 under the supervision of Prof. Shi-Gang Sun. He is a joint Ph.D. student at Lawrence Berkeley National Lab (U.S.) between 2016 and 2019 under the supervision of Prof. Haimei Zheng. Dr. Yin is currently a postdoctoral at the School of Advanced Materials, Peking University Shenzhen Graduate School. His research interests mainly focus on the electrochemical reaction mechanisms in batteries, catalysis, and advanced characterization techniques, such as EQCM, TEM, XAS, etc.

www.advancedsciencenews.com www.afm-journal.de



Wenguang Zhao is an engineer in the School of Advanced Materials, Peking University Shenzhen Graduate School, China. He has over ten years of experience in material characterization using a wide range of analytical tools including TEM, XRD, XPS, and SEM. His research interests mainly focus on the ex/in situ TEM and ex/in situ XRD characterization of battery materials.



Jianyuan Li received his B.S. degree from the School of Chemistry and Chemical Engineering, Shandong University, China in 2017. He is currently a Ph.D. candidate in School of Advanced Material, Peking University, China. His research interests focus on the structure evolution and characterization of battery materials.



Xin-Xing Peng received his B.S. degree in 2014 and Ph.D. degree in 2019 from Xiamen University under supervision of Prof. Shi-Gang Sun. His research is mainly focused on battery materials charracterization and in situ TEM.



Cong Lin received his B.S. and Ph.D. degree in Chemistry from Chongqing University and Peking University in 2013 and 2018, respectively. From 2018 to early 2021, he worked as a postdoctoral in Prof. Feng Pan's group in Peking University Shenzhen Graduate School, and is currently a postdoctoral fellow in The Hong Kong Polytechnic University. His research interest mainly focuses on the structures of novel functional materials and their relationship with properties and performances.

16163028, 2022, 1, Downloaded from https://advanced.onlinelibrary.wiley.com/doi/10.1002/adfm.202107190 by University Town Of Shenzhen, Wiley Online Library on [24/11/2025]. See the Terms and Conditions (https://onlinelibrary.wiley

and-conditions) on Wiley Online Library for rules of use; OA articles are governed by the applicable Creative Commons



Mingjian Zhang got his Ph.D. degree from Fujian Institute of Research on the Structure of Matter, Chinese Academy of Sciences in 2013, then worked there as an assistant research fellow for one year. From 2014 to 2018, he was a postdoc in School of Advanced Materials, Peking University, and became an assistant research professor in 2018–2020, and promoted to an associate research professor since 2021. Meanwhile, he was a research scholar in Brookhaven National Lab from 2016 to 2019, then in the University of Chicago in 2019. He has been engaged in the fields of high-performance cathode materials for Li-ion batteries, especially the structural evolution and structure-property research of the cathodes.



Zhiyuan Zeng obtained his B.E. and M.E. from Central South University, Zhejiang University in 2006 and 2008, respectively. He completed his Ph.D. with Prof. Hua Zhang at Nanyang Technological University, Singapore (2013). He joined Dr. Haimei Zheng's group as a Postdoctoral Fellow at Lawrence Berkeley National Laboratory (2013–2017). After working for Applied Materials Inc. in Silicon Valley (2017–2019), he joined City University of Hong Kong as an assistant professor in 2019. His research interest focuses on transition metal dichalcogenides and transition metal oxides based materials for energy and environmental applications.



Hong-Gang Liao is a professor at College of Chemistry and Chemical Engineering in Xiamen University, China. He received his Ph.D. degree in Physical Chemistry from Xiamen University. From 2011 to 2015, he works as a Research associate in Lawrence Berkeley National laboratory in Haimei Zheng's group, one of the leading groups in the liquid phase TEM. Currently, his research focuses on 1) the development of in situ TEM techniques. Combine the advanced nanofabrication technology with electron microscopy to enable atomic scale imaging in liquids under biasing, heating or light illumination. 2) By using liquid phase TEM, addressing fundamental issues in materials, chemistry, energy storage, and conversion



Haibiao Chen is currently a research professor at Shenzhen Polytechnic. He received his bachelor's degree from Tsinghua University in 2000 and Ph.D. from Stevens Institute of Technology in 2006. He worked at Velocys during 2006–2011 and UES during 2011–2014. He was a senior researcher at the School of Advanced Materials, Peking University Shenzhen Graduate School from 2014 to 2020.

16163028, 2022, 1, Downloaded from https://advanced.onlinelibrary.wiley.com/doi/10.1002/adfm.202107190 by University Town Of Shenzhen, Wiley Online Library on [24/1/2025]. See the Terms

conditions) on Wiley Online Library for rules of use; OA articles are governed by the applicable Creative Commons

www.advancedsciencenews.com www.afm-journal.de



Hai Lin is a vice dean of School of Advanced Materials, Peking University Shenzhen Graduate School. He is responsible for the testing and characterization platform of new materials, and focusing on the evaluation and industrial application development of clean energy materials and devices



Feng Pan is a chair professor, VP Peking University Shenzhen Graduate School, founding dean of School of Advanced Materials, director of National Center of Electric Vehicle Power Battery and Materials for International Research, received his B.S. degree from Department of Chemistry, Peking University in 1985 and Ph.D. from Department of P&A Chemistry, University of Strathclyde, U.K. with "Patrick D. Ritchie Prize" for the best Ph.D. in 1994. Prof. Pan has been engaged in fundamental research of structure chemistry, exploring "Material Gene" for Li-ion batteries and developing novel energy conversion-storage materials & devices. He also received the 2018 ECS Battery Division Technology Award (US), and 2021 China Electrochemistry Contribution Award.